


# APEX2-mediated RAB proximity labeling identifies a role for RAB21 in clathrin-independent cargo sorting

Tomas Del Olmo<sup>1</sup>, Annie Lauzier<sup>1</sup>, Caroline Normandin<sup>1</sup>, Raphaëlle Larcher<sup>1</sup>, Mia Lecours<sup>1</sup>, Dominique Jean<sup>1</sup>, Louis Lessard<sup>1</sup>, Florian Steinberg<sup>2</sup>, François-Michel Boisvert<sup>1</sup> & Steve Jean<sup>1,\*</sup> 

## Abstract

RAB GTPases are central modulators of membrane trafficking. They are under the dynamic regulation of activating guanine exchange factors (GEFs) and inactivating GTPase-activating proteins (GAPs). Once activated, RABs recruit a large spectrum of effectors to control trafficking functions of eukaryotic cells. Multiple proteomic studies, using pull-down or yeast two-hybrid approaches, have identified a number of RAB interactors. However, due to the *in vitro* nature of these approaches and inherent limitations of each technique, a comprehensive definition of RAB interactors is still lacking. By comparing quantitative affinity purifications of GFP:RAB21 with APEX2-mediated proximity labeling of RAB4a, RAB5a, RAB7a, and RAB21, we find that APEX2 proximity labeling allows for the comprehensive identification of RAB regulators and interactors. Importantly, through biochemical and genetic approaches, we establish a novel link between RAB21 and the WASH and retromer complexes, with functional consequences on cargo sorting. Hence, APEX2-mediated proximity labeling of RAB neighboring proteins represents a new and efficient tool to define RAB functions.

**Keywords** APEX2; clathrin-independent endocytosis; RAB GTPases; retromer; WASH complex

**Subject Categories** Membrane & Intracellular Transport; Methods & Resources

**DOI** 10.15252/embr.201847192 | Received 5 October 2018 | Revised 6 December 2018 | Accepted 10 December 2018

**EMBO Reports (2019) e47192**

## Introduction

Membrane trafficking, the vesicular transport of cellular constituents, is fundamental to cellular and organismal homeostasis [1–3]. The sequential transport of cargos between intracellular compartments occurs through multi-step processes that are actively regulated [4]. One important class of regulators controlling vesicular

traffic and membrane compartment identity is the RAB GTPase family [5].

RAB GTPases form the largest family of small GTPases with nearly 70 members in humans [6]. RABs are involved at every step of vesicular trafficking where they regulate sorting, fission, transport, tethering, and fusion events [7]. RABs cycle between their inactive (GDP-bound) and active (GTP-bound) states through the action of guanine exchange factors (GEFs), and are conversely converted from their GTP-bound state to their GDP state by GTPase-activating proteins (GAPs) [8]. RABs are often targeted by multiple GEFs and GAPs [9,10]. The differential actions of these GEFs or GAPs can potentially direct a RAB to alternate compartments or specify particular functions [11]. Once recruited and activated at their target membranes, RABs bind effectors in order to mediate various functions [12]. RAB effectors recruit multiple classes of proteins ranging from adaptor coat proteins to myosins, dyneins, and signaling kinases [12]. Moreover, RABs also interact with various cargos, tethering complexes and cargo sorting complexes [13]. One such example is the role of RAB7 in the recruitment of the retromer complex at endosomes [13,14]. The retromer complex is an evolutionary conserved complex [15], which regulates endosome-to-Golgi retrograde transport [16] as well as endosome-to-plasma membrane trafficking [17]. The core retromer complex is constituted of two subcomplexes, namely the VPS and SNX complexes. The VPS complex (or cargo sorting complex) comprises VPS26, VPS29, and VPS35 [18] and interacts with various cargos either directly or through binding with various SNXs and accessory proteins [17,19,20]. The SNX subcomplex interacts with endosomes through PtdIns(3)P [21] and also modulates cargo sorting [22,23] as well as membrane tubulation [24]. In addition, the retromer interacts with the WASH complex, through an interaction between VPS35 and the WASH complex subunit FAM21 [19,25,26]. The WASH complex generates F-actin at endosomes to mediate cargo sorting and tubule scission [27–30]. It is now acknowledged that the retromer/WASH complex forms heterogeneous “subcomplexes” with various interacting proteins to specifically and temporally regulate a large array of cargos [17,20,31–33]. Given the role of RAB

<sup>1</sup> Faculté de Médecine et des Sciences de la Santé, Département d'Anatomie et de Biologie Cellulaire, Université de Sherbrooke, Sherbrooke, QC, Canada

<sup>2</sup> Center for Biological Systems Analysis (ZBSA), Faculty of Biology, Albert Ludwigs Universitaet Freiburg, Freiburg, Germany

\*Corresponding author. Tel: +1 819 821 8000; Fax: +1 819 820 6831; E-mail: steve.jean@usherbrooke.ca

GTPases in membrane traffic, it is likely that other RABs are involved in various aspects of retromer/WASH functions.

RAB interactors have mostly been defined through *in vitro* pull-down and yeast two-hybrid approaches [34–37]. Pull-down experiments are a powerful tool to assess direct binding between a RAB and a specific protein, and have been successfully used to identify interactors for multiple RABs [35]. However, they preclude identification of context-specific RAB GEFs, GAPs, or effectors, since the temporal aspects of effector recruitment are lost. On the other hand, yeast two-hybrid approach allows for the identification of RAB GEFs, GAPs, and effectors. However, yeast two-hybrid approach only monitors binary interactions, and as a result, complexes interacting with RABs through multiple proteins cannot be identified. Recently, a pull-down-based RAB-interactome screen was performed in *Drosophila* enabling identification of a large number of RAB effectors [37]. Unfortunately, harder to purify RABs showed very limited number of interactors [37]. Ongoing proteome-wide studies aimed at defining the human proteome [38] have also tested numerous RAB GTPases. Unfortunately, these studies used C-terminal tags for affinity purifications, which are not appropriate for RABs, due to RAB C-terminal prenylation. The suboptimal tagging of the RABs in these studies yielded a low number of interactors for most of the twenty-five RABs tested. This was particularly evident given the strong prevalence for enzymes linked to RAB prenylation in the interactome (i.e., CHM, CHML, RABGGTA/B) [38]. Hence, in order to understand how RABs exhibit different cellular functions, it is imperative to accurately and extensively define their associated proteome in the appropriate setting. In an effort to develop new approaches to map RAB GTPase interactors, we have combined quantitative mass spectrometry and APEX2 proximity labeling techniques. Herein, we describe APEX2-mediated proximity labeling as a new highly efficient method to rapidly map RAB regulators/effectors. This approach notably allowed defining a novel RAB21 interaction with the WASH/retromer complexes and a RAB21 role in endosomal sorting of a subset of clathrin-independent cargos.

## Results

### Quantitative mass spectrometry defines potential RAB interactors

Early endosomal RAB21 has well-described roles in mediating integrin internalization to control cell migration, anoikis resistance, and cell division [39,40]. RAB21 also regulates aspects of VAMP7 and VAMP8 trafficking to control neurite growth and autophagy, respectively [41,42]. Unfortunately, a low number of specific interactors were identified for RAB21 in a recent pull-down study [37]. Given the importance of RAB21-associated functions, and the difficulty in identifying RAB21 interactors through conventional approaches, RAB21 represents a good RAB on which to establish novel methodologies aimed at identifying RAB-associated proteins. Hence, a quantitative SILAC-based affinity purification (AP-MS) approach was devised to map RAB21 interactors.

The Flp-In/T-REx system [43] was used to generate stable HeLa and HCT116 cell lines expressing N-terminally GFP-tagged wild-type (WT), GTP-locked (Q78L), or GDP-locked (T33N) forms of human

RAB21. Various RAB21 variants were chosen in order to maximize the recovery of GEFs, GAPs, and effectors. GFP:RAB21 variants were expressed and properly localized in both HeLa and HCT116 cells, except for T33N that showed weaker early endosomal localization with a concomitant Golgi relocalization (Fig EV1A–D), consistent with earlier findings [44].

Duplicate SILAC experiments for each GFP:RAB21 variants identified a vast spectrum of potential direct and indirect RAB21 interactors (Figs EV1E and EV2A–C, Dataset EV1). Surprisingly, functional annotations in Reactome of individual cell lines did not show an enrichment toward membrane trafficking (Fig EV2D and E) and were reminiscent of those observed from a recently published GST:RAB21-interactome pull-down study (Fig EV2F) [45]. Since the interactome was generated in two cell lines, we hypothesized that proteins concomitantly enriched from both cell lines would likely represent RAB21 interactors. Hence, the HeLa and HCT116 RAB21 networks generated with all of the various RAB21 variants were merged. This resulted in 29 proteins present altogether (Fig EV1E), which interacted to different degrees with the WT, Q78L, or T33N RAB21 variants (Fig EV2C and Dataset EV1). When organized into a network (Fig EV1F), multiple membrane trafficking regulators or potential cargos were observed. Reactome pathway analysis revealed an enrichment in membrane and vesicular transport processes (Fig EV1G), strengthening these core proteins as prospective RAB21 interactors. While this quantitative AP-MS interactome yielded a highly relevant network of RAB21 binding proteins, it was nonetheless variable between repeats and cell lines and required the use of GDP-/GTP-locked constructs. Therefore, other approaches were sought to identify RAB regulators and interactors.

### APEX2:RABs are properly localized in HeLa cells

One caveat of AP-MS and pull-down approaches is that cell lysis influences protein–protein interactions. To circumvent this issue, APEX2:RAB fusions were used to perform proximity labeling (Fig 1A) [46]. APEX2 is an engineered peroxidase that biotinylates proteins, mostly on tyrosine [47], in a 10–20 nm radius [48]. It uses biotin–phenol as its substrate, and the reaction is catalyzed by a 1-min H<sub>2</sub>O<sub>2</sub> treatment, enabling the rapid covalent labeling of neighboring proteins.

A concern with proximity labeling approaches is that they often lead to the identification of large arrays of proteins [49]. We rationalized that by using three early endosomal RABs as baits, we could (i) validate the technique, (ii) identify general and specific early endosomal neighbors for the three RABs, and (iii) refine the RAB21 proteome established by AP-MS. Moreover, given the known segregation of RAB5 and RAB4 at endosomes [50,51], we hypothesized that APEX2 labeling would also identify RAB-specific microdomains (Fig 1B). APEX2, APEX2:RAB21, APEX2:RAB5a, and APEX2:RAB4a HeLa Flp-In/T-REx cells were thus generated. APEX2-fused RABs were able to biotinylate endogenous proteins. Strong biotinylation was observed in the presence of H<sub>2</sub>O<sub>2</sub> and biotin–phenol, whereas weak biotinylation was noted when H<sub>2</sub>O<sub>2</sub> was omitted (Fig 1C). Immunofluorescence analyses revealed that biotinylated proteins in APEX2:RAB21, RAB5, and RAB4 cells localized on EEA1-positive puncta and also in a cytosolic/reticular pattern, while APEX2-only cells showed diffuse cytosolic and nuclear staining with no EEA1 colocalization (Fig 1D). Together, these results indicate

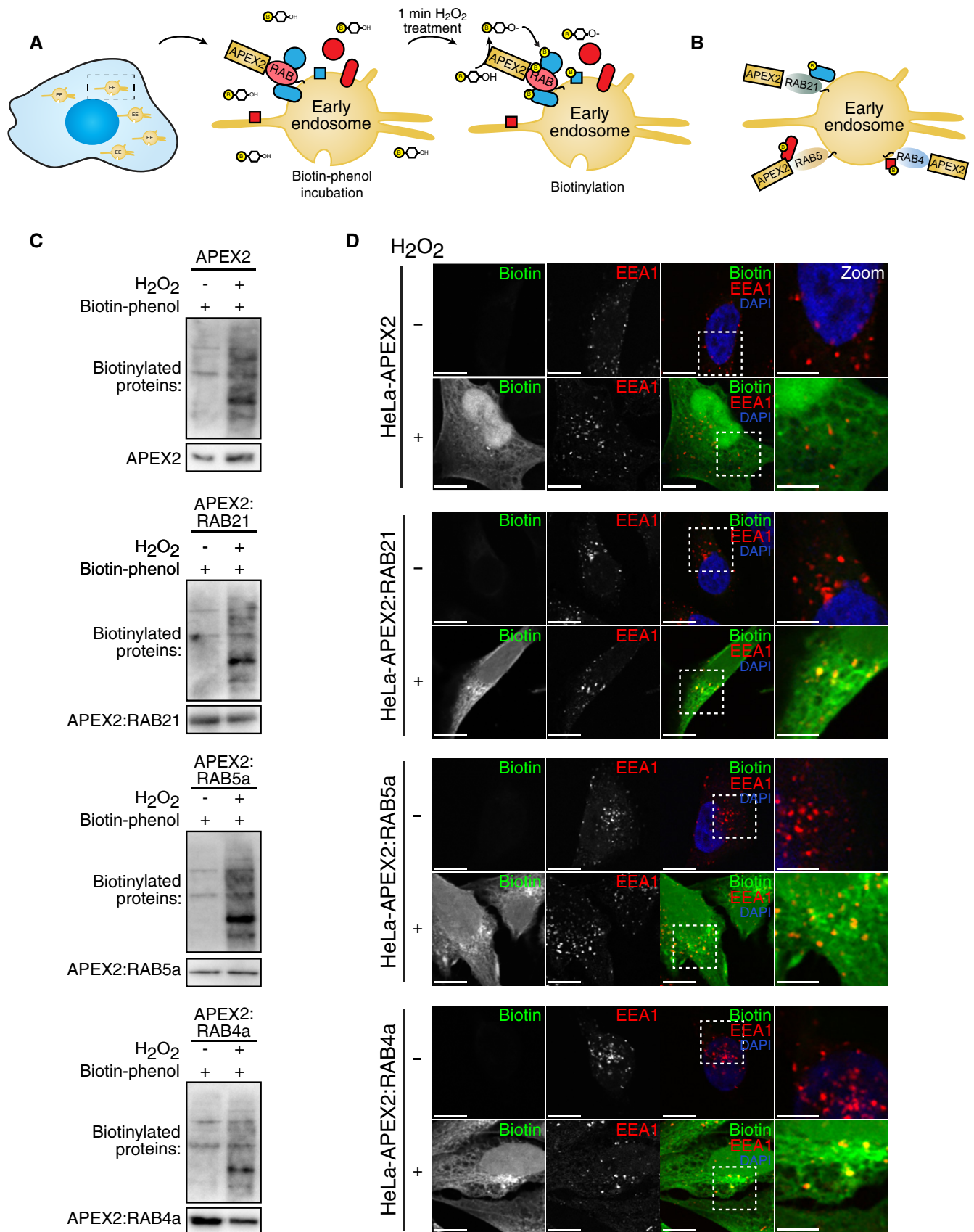


Figure 1.

**Figure 1. APEX2:RAB expression lead to endosomal biotinylation.**

- A Diagram representing APEX2:RAB-mediated endosomal biotinylation of endogenous proteins.  
 B Illustrative representation of APEX2:RAB endosomal microdomains.  
 C APEX2 only or APEX2:RAB were found to biotinylate endogenous proteins. Streptavidin Western blotting of total biotinylated proteins in APEX2:RAB or APEX2 only Flp-In/T-REx HeLa cells.  
 D APEX2:RAB biotinylated proteins (streptavidin) are partially colocalized with EEA1 in HeLa cells,  $n = 2$  independent experiments. Scale bars: 10  $\mu\text{m}$  or 5  $\mu\text{m}$  in enlarged views.

that APEX2 is active when fused with RABs and that APEX2:RAB can biotinylate proteins at EEA1-positive endosomes.

**APEX2:RAB proximity labeling is enriched for trafficking regulators/ effectors**

Three label-free independent proximity labeling experiments for each RABs and the APEX2 control were performed. In order to statistically identify interactors/neighbors and to remove cytosolic/reticular contaminants, the SAINT software was used for filtering and the ProHits-viz suite for data representation [52,53]. Using a very strict SAINT filtering score of  $\geq 0.95$ , which corresponds to a false discovery rate of  $\leq 1\%$ , 1,173 proteins were identified in APEX2:RAB21, 819 in APEX2:RAB5, and 469 in APEX2:RAB4 when normalized to APEX2 only (Fig 2A and Dataset EV2). Importantly, biotinylation was equivalent between APEX2:RABs (Fig EV3A). Therefore, the different number of interactors/neighbors between the various RABs most probably reflects different degrees of proximity with endosomal proteins, rather than variable protein expression levels between baits. RAB5 and 21 showed 57% overlap between their neighboring proteins (666 proteins), while RAB21/RAB4 and RAB5/RAB4 had 35% (412 proteins) and 51% overlap (415 proteins), respectively (Fig 2A). When all RAB21, RAB5, and RAB4 neighbors were analyzed for gene ontology (GO) term enrichment, molecular functions related to trafficking events were highly significant and overlapped extensively (Fig 2B). Of significance, the APEX2:RAB approach highlighted cellular functions related to trafficking, something that both GST pull-down and AP-MS approaches failed to achieve without heavy filtering and the use of numerous RAB variants and cell lines.

**Wild-type APEX2:RABs identify known GEFs, GAPs, and effectors**

Given the large number of proteins identified in the APEX2:RAB21, 5, and 4 datasets, the type of neighbors detected through this methodology was explored. A comparative analysis of the various RABs (Fig 2C) on ProHits-viz was performed. Strikingly, GEFs, GAPs, and effectors/interactors were identified from wild-type RABs with mostly specific enrichments toward their predicted target. Using published interactors (without exhaustively listing them all, Fig 2C and Dataset EV2), preferential associations between RAB21 and MTMR2 were observed, as shown in *Drosophila* [54] and with VAMP7 [41]. An association between RAB21 and integrin(s) was also detected, although integrins were rather variable in their proximity with early endosomal RABs, as could be expected from previous reports [55]. APPL1/2 and EEA1, which are known RAB21 and RAB5 effectors, were also highly recovered with both RAB21 and RAB5, while weak in RAB4. APEX2:RAB5-mediated proximity ligation also identified other known RAB5 effectors, including VPS34 and KIF13A. It also enriched HOOK1/3, UHRF1BP1L, CC2D1A,

FAM160A1, and Ccdc128, which represent previously identified RAB5 effectors [37]. Surprisingly, Rabenosyn-5, which binds both RAB5 and 4, was mostly enriched with RAB5 compared to RAB4. RABIP4, RAB11FIP11, and VPS45, which are functionally mostly linked to RAB4, were also more prominently found with RAB5 or RAB21 compared to RAB4, while only GRASP-1 was notably observed with RAB4. Nonetheless, all of these known RAB4 interactors, although less abundant with RAB4, were recovered at an  $< 1\%$  FDR in APEX2:RAB4 experiments.

The APEX2 approach also identified known RAB21 and RAB5 GEFs (Fig 2C). VARP, a RAB21 GEF, was highly abundant with RAB21, while the more general RABGEF1 was observed at a low FDR ( $< 1\%$ ) with RAB21 and 5. RAB GAPs were also recovered by APEX2:RABs (Fig 2C). Of note, TBC1D2, previously described with RAB5 GAP activity in *C. elegans* [56], was abundant with RAB5, while GAPCENA, a known RAB4 GAP, was present with RAB4 [57]. No RAB21 GAPs have been described in the literature, although TBC1D17 was shown to have weak catalytic activity toward RAB21 *in vitro* [57]. TBC1D4 and/or TBC1D15, a close relative of TBC1D17, could potentially act on RAB21 given their respective high abundance with RAB21.

To confirm that APEX2:RAB-identified proteins were recovered due to their close proximity to RABs, and not merely the result of their general endosomal localization, the RAB21 dataset was compared to a previously published APEX2:2xFYVE dataset [58]. The data were normalized using ProHits-viz and compared. After analysis, most proteins were only found with RAB21 (Fig EV3B), while those shared between the 2xFYVE probe and RAB21 were, for the most part, known PtdIns(3)P binding or associated proteins (Fig EV3C). Thus, proteins identified through APEX2:RAB were not simply observed due to their endosomal localization. To further ensure the specificity of the APEX2:RAB-identified proteins, early endosomal RABs were compared to APEX2:RAB7a, a late endosomal RAB. APEX2:RAB7 localized appropriately and led to biotinylation at late endosomes/lysosomes as detected with LAMP1 (Fig EV3E). APEX2:RAB7-identified proteins had a limited overlap with early endosomal RABs as expected (Figs 2A–C and EV3D). Importantly, the well-described RAB7 GAP TBC1D5 [14] and the known RAB7 interactor VPS35 [59] were highly enriched with RAB7 (Fig 2C). Altogether, these experiments strengthen APEX2:RAB proximity labeling as an efficient method to identify RAB interactors/neighbors.

Another important aspect of the APEX2:RAB proximity labeling approach was that it successfully enriched whole protein complexes with single RABs (Fig 2C). This approach, using a single purification step, effectively identified all subunits of the EARP complex with RAB4. This complex was recently identified as an early endosomal sorting complex interacting with RAB4 [60,61]. EARP is highly similar to the Golgi GARP complex, which does not interact with RAB4 [37]. Of note, all EARP-specific subunits were identified with strong

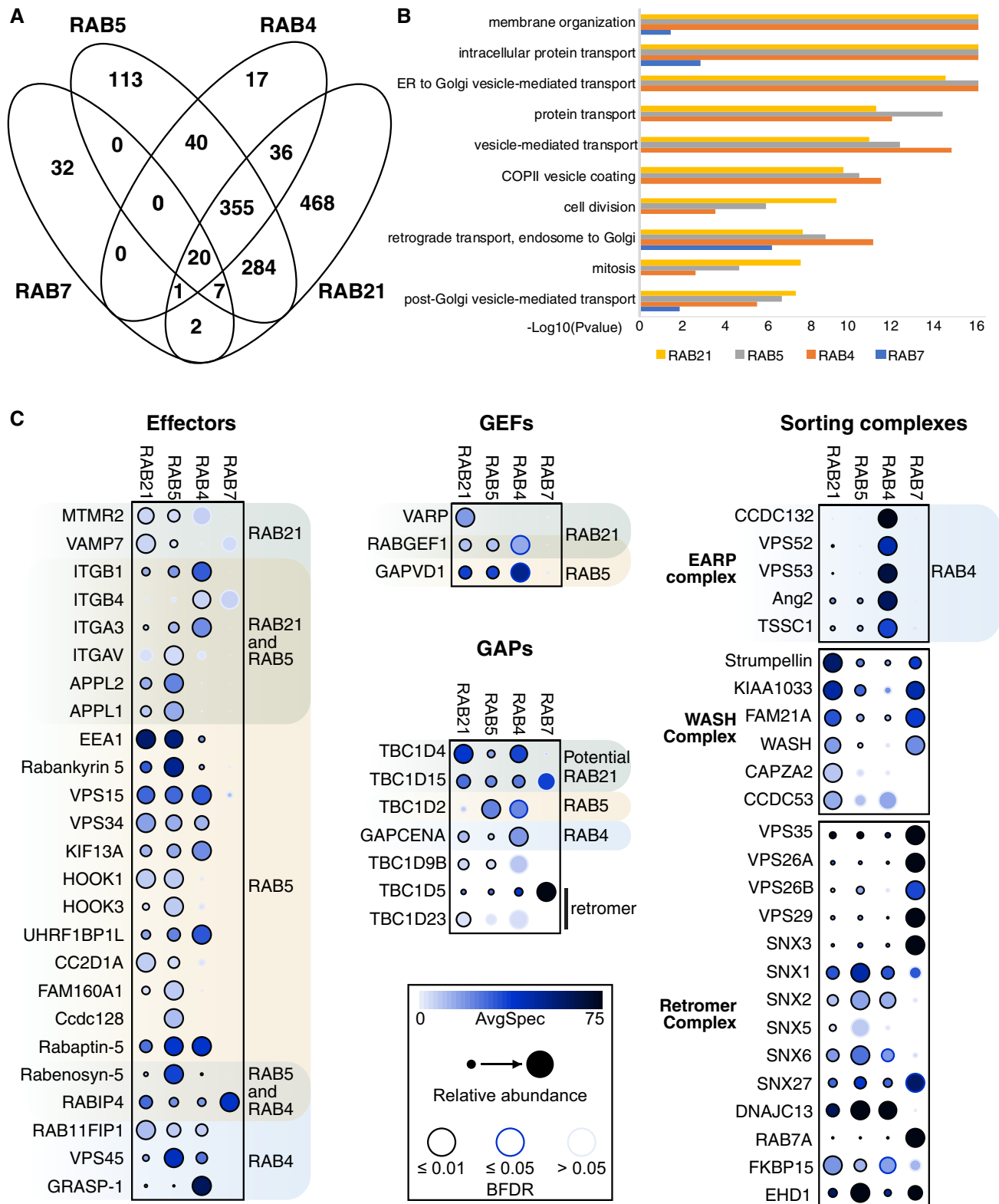


Figure 2. Comparison of APEX2:RAB21-, 5-, 4-, and 7-generated proteomes.

A Venn diagram highlighting the number of interactors with each RAB and their overlap.

B Reactome analysis of all APEX2:RAB21, APEX2:RAB5, APEX2:RAB4, and APEX2:RAB7 interactors/neighbors.

C ProHits-viz generated dot plots of RAB effectors, GEFs, GAPs, and sorting complexes. Green, blue, and beige shadings along with RAB names refer to previously identified interactions between RABs and the depicted proteins.

enrichment with RAB4, while the GARP complex-specific subunit was not recovered. Also, the WASH [62] complex was strongly enriched with RAB21, while a few subunits were observed with RAB5 and RAB7 (Fig 2C). Interestingly, VPS retromer subunits [18] were strongly enriched with RAB7, compared to early endosomal RABs (Fig 2C), as expected from previous work [13,14]. Although early endosomal RABs were statistically enriched with the VPS retromer subunit, they showed stronger proximities to various SNXs and other retromer subunits (i.e., SNX2, SNX6).

RAB GTPases are known to be functionally linked to phosphoinositides [5]. Thus, their proximity to phosphoinositide regulatory enzymes was investigated. RAB21 and RAB5 were found to interact or be in close proximity to a wide range of phosphoinositide phosphatases and kinases (Fig EV4A). In accordance with previous studies [63], APEX2 proximity labeling identified INPP4a and OCRL as strong RAB5 interactors/neighbors. Interestingly, multiple Myotubularin family members were specifically identified with RAB21. Moreover, PIKFYVE was also exclusively found in APEX2:RAB21 cells (Fig EV4A). These associations imply that RAB21 could potentially impact three phosphoinositide pools, namely PtdIns(3)P, PtdIns(5)P, and PtdIns(3,5)P<sub>2</sub>. Altogether, APEX2:RAB proximity labeling allowed identifying a wide array of known regulators/interactors of RAB GTPases.

#### APEX2:RABs identify novel RAB interacting proteins

Most of the aforementioned proteins represent known interactions and complexes. Consequently, the extent of the interactors/neighbors identified by the APEX2 technique validated the APEX2 approach. However, in addition, we also assessed whether APEX2:RABs proximity labeling could identify novel regulatory interactions. In order to identify RAB21 interactors/neighbors, APEX2:RAB21 enriched baits were filtered (Fig EV4B). This led to the identification of (i) PLEKHM2, which has known roles in lysosomal positioning and autophagy [64], (ii) SLC7A11, which interacts with SLC3A2 to control amino acid transport [65], and (iii) USP7, a recently identified WASH complex modulator [66]. Other identified RAB21 interactors/neighbors showed potential roles in TGF- $\beta$ , in adherent junctions, and in cohesin functions. To assess whether proteins detected by mass spectrometry could be validated by other approaches, APEX2 and APEX2:RAB21 proximity labeling in GFP:SARA transfected cells was performed. After cell lysis and GFP:SARA immunoprecipitation, biotinylated SARA was only observed in APEX2:RAB21 cells (Fig EV4C). Moreover, co-immunoprecipitation (CoIP) experiments performed between FLAG:RAB21WT- and HA:PLEKHM2- or HA:SLC7A11-expressing cells allowed highlighting reproducible interactions between RAB21 and PLEKHM2 or SLC7A11 (Fig EV4D). These examples further strengthen the APEX2 proximity labeling technique and corroborate these newly established neighbors as novel RAB21 interactors.

#### RAB21 interacts and colocalizes with the WASH and retromer complexes

In order to further build from the APEX2 proximity labeling approach and define novel molecular functions for RAB21, its proximity to the WASH and retromer complexes was studied in further detail. Mass spectrometry data were confirmed by performing an

anti-biotin immunoprecipitation [67] on APEX2:RAB-expressing cells, and the presence of WASH- and retromer-associated proteins was tested. Using this approach, Strumpellin was more prevalent with APEX2:RAB21, while similar amounts of VPS35 between RAB5 and RAB21 (Fig 3A) were detected. This trend is in accordance with the mass spectrometry approach (Fig 2C).

Specific interactions between RAB21 and WASH/retromer complexes subunits were further tested by CoIP. Endogenous VPS26, FAM21, Strumpellin, and VPS35 immunoprecipitated with GFP:RAB21 (Fig 3B and C). Although weak, these interactions were highly reproducible and associated with different degrees with the various RAB21 variants. This is similar to RAB21 association with integrins [68]. Of particular note, VPS35 was also observed in the AP-MS SILAC experiments (Dataset EV1). Lastly, pull-down experiments on HeLa cell lysates with bacterially purified GST:RAB21 [54] were performed to assess a more direct interaction between the WASH/retromer complexes and RAB21. FAM21, Strumpellin and CAPZ $\alpha$ , three WASH complex components, and VPS35, a core retromer subunit (Fig 3D), were detected. The efficiency of the pull-down was confirmed by the presence of APPL1 (Fig 3D). While these pull-down results do not allow concluding that RAB21 directly interacts with the WASH or retromer complexes, they nevertheless strongly suggest that RAB21 binds to these complexes either directly or indirectly. Finally, as expected from the interaction data, partial colocalization between RAB21 and the WASH and retromer complexes was observed (Fig 3E and F), further indicating that RAB21 interacts with the WASH and retromer complexes.

#### RAB21 is required for complete endosomal WASH/retromer complex recruitment

To functionally assess whether RAB21 affects WASH/retromer functions, polyclonal RAB21 knockout HeLa cell populations were generated using CRISPR/Cas9 [69]. To ensure the specificity of the assayed phenotypes, two cell populations using independent guide RNAs targeting distinct genomic regions were generated. Thus, similar phenotypes in both cell populations would strongly argue for a specific effect. RAB21 knockout was confirmed through sequencing of the targeted genomic regions, with various indels or insertions observed for each gRNA in the polyclonal populations (Fig EV4E). Some non-edited cells were observed in the gRNA-2 cell population compared to the gRNA-3 population (Fig EV4E), which correlated with RAB21 protein levels detected by Western blotting (Fig 4A). Importantly, as expected from previous studies [42], the number of LC3 puncta was increased in the two RAB21 knockout cell populations (Fig EV4F). Morphological analysis of various membrane compartments did not identify major defects in compartment size and localization (Fig 4B), aside from transferrin uptake being slower in RAB21 KO cells (Fig EV4G and H) in accordance with previous work [44].

RAB21 knockout led to a slight reduction in VPS35 and VPS26 protein levels, while it did not affect VPS29. On the opposite, WASH, Strumpellin, and CAPZ $\alpha$  proteins levels showed a slightly increasing trend (Fig 5A and B), indicating that RAB21 may regulate the localization or stability of these complexes. Significantly, loss of RAB21 reduced VPS35 recruitment to endosomes detected both by a decreased number of VPS35 puncta per cells and by a reduced colocalization between VPS35 and EEA1 (Fig 5C–E). Decreased

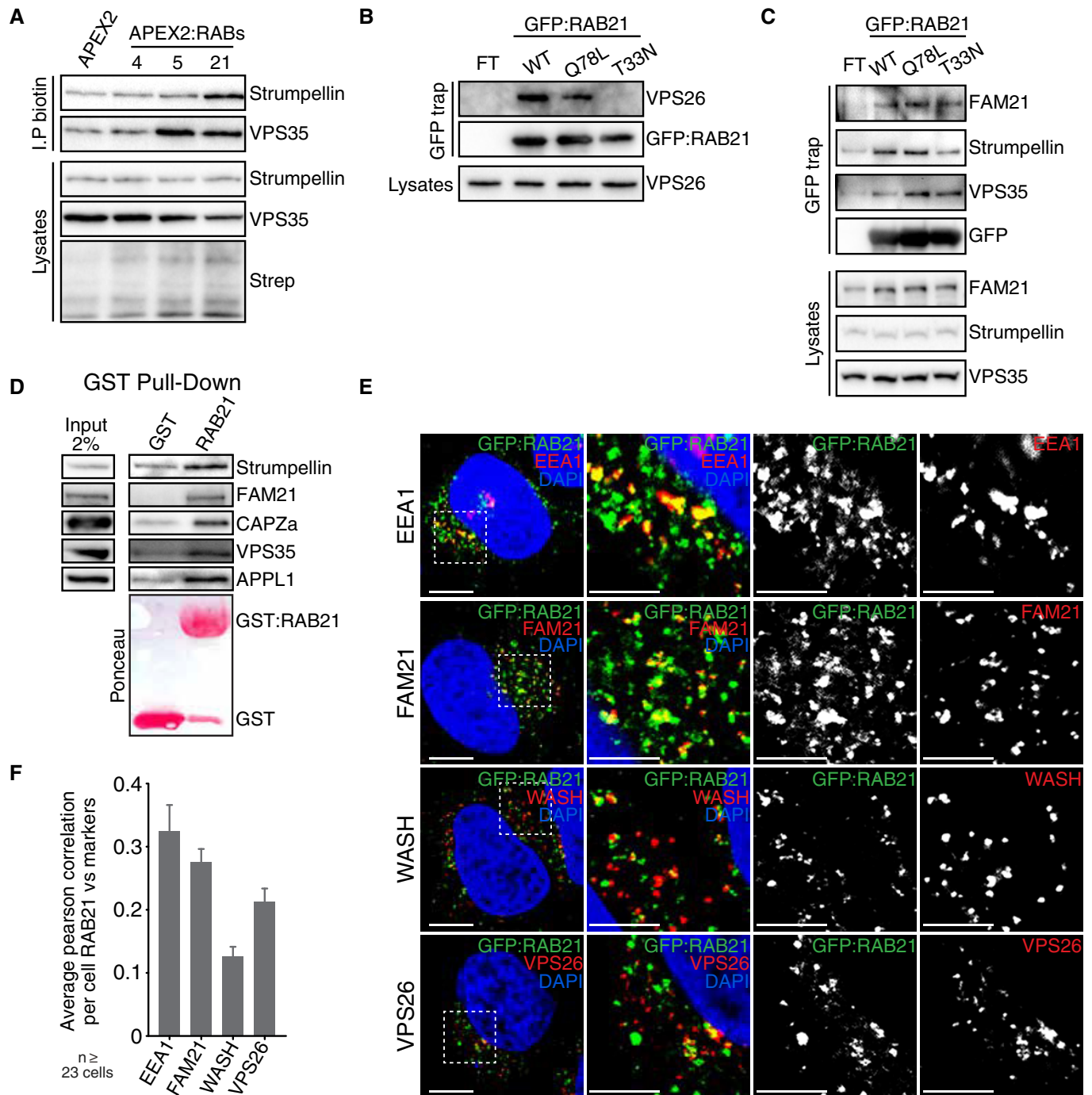


**Figure 3. RAB21 interacts and colocalizes with the WASH and retromer complexes.**

- A** Strumpellin and VPS35 are in close proximity to RAB5 and RAB21. Anti-biotin immunoprecipitation and immunoblot of endogenous Strumpellin and VPS35. Lysates correspond to 1% of input,  $n = 3$  independent experiments.
- B, C** RAB21 can be seen interacting with various WASH and retromer complexes subunits. GFP-Trap IP of WT, Q78L, and T33N RAB21 variants in HeLa cells followed by GFP immunoblot and endogenous (B) VPS26 immunoblot and (C) FAM21, Strumpellin, and VPS35 immunoblots. Lysates correspond to 5% of input,  $n \geq 3$  independent experiments.
- D** RAB21 actively pulls down WASH and retromer complex subunits. Bacterially purified and GTP-loaded GST:RAB21 pull-down of HeLa cell lysates followed by Strumpellin, FAM21, CAPZ $\alpha$ , and VPS35 immunoblots. Ponceau staining reveals the purity of the GST and GST:RAB21 used for the pull-downs,  $n = 3$  independent experiments.
- E** RAB21 colocalizes with the WASH and retromer complexes. Transiently expressing GFP:RAB21 HeLa cells were fixed and stained for endogenous EEA1, FAM21, WASH, and VPS26. Boxed region is magnified, and single channels are depicted. Scale bars: 10  $\mu\text{m}$  or 5  $\mu\text{m}$  in enlarged view.
- F** Pearson's correlation per cell between RAB21 and the various markers. Error bars are SEM,  $n = 2$  independent experiments.

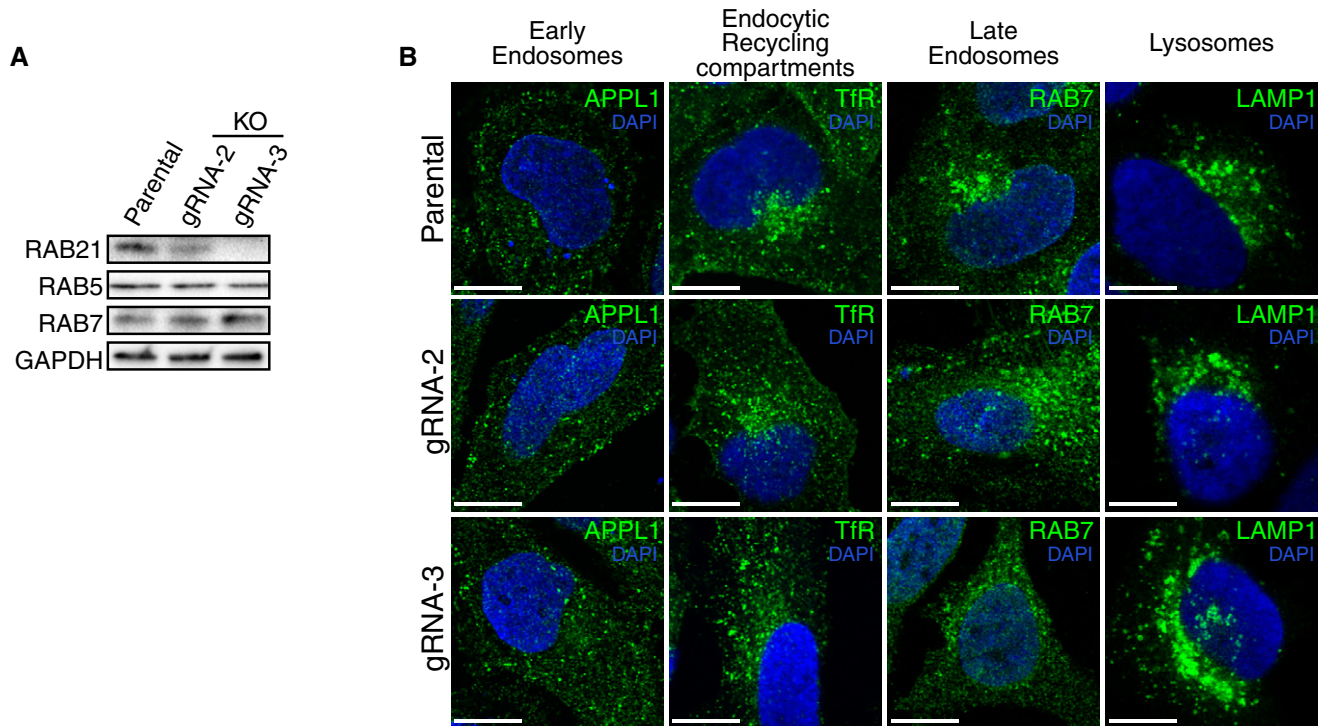


**Figure 4. Characterization of RAB21 knockout HeLa cells.**

**A** Low RAB21 expression levels in two independent RAB21 KO cell populations. Immunoblot analysis of endogenous RAB21, RAB5, RAB7, and GAPDH.

**B** Endo-lysosomal compartments are unaffected by the loss of RAB21. Immunofluorescence of APPL1, TfR, RAB7, and LAMP1 in parental HeLa cells and in the two RAB21 knockout cell populations. Scale bars: 10  $\mu$ m,  $n = 3$  independent experiments.

colocalization between SNX1 and EEA1 was also observed, although the number of endosomal SNX1 puncta was not affected by RAB21 deletion (Fig EV5A–C), suggesting that the cargo sorting complex is more affected by the loss of RAB21 than the sorting nexin complex. WASH and FAM21 also showed, albeit to a weaker extent than VPS35, decreased endosomal colocalization with EEA1 (Figs 5F–H and EV5D). Altogether, these results demonstrate that RAB21 is required for the full recruitment of the WASH and retromer complexes at EEA1-positive endosomes. To assess whether RAB21 was required for a specific WASH-mediated process, endosomal F-actin was monitored since it is believed to be mostly controlled by the WASH complex [27,28,70]. Importantly, endosomal F-actin was decreased in RAB21 KO cells compared to controls (Fig 5I and J) demonstrating the importance of RAB21 for proper WASH function. This was not a global loss of F-actin, since cortical actin was present equally in parental and RAB21 knockout cells (Fig 5I).

#### RAB21 regulates trafficking of a subset of retromer cargos

The interaction and impact of RAB21 on WASH/retromer localization and actin polymerization suggest that RAB21 may regulate the trafficking of a larger proportion of cargos than initially believed [39,42]. WASH/retromer complexes regulate endosome-to-Golgi retrograde pathways and cargo recycling between endosomes and plasma membrane [17,29]. Thus, given that both CI-MPR and GLUT1 proteins represent two well-defined retromer cargos undergoing retrograde or endosome-to-plasma membrane

sorting, respectively [17,71], the localization of these two proteins was therefore assessed. Surprisingly, in RAB21 knockout cells, no defects were observed for either cargos (Fig 6A–C), thereby indicating that RAB21 is not required for general retromer sorting events, and consistent with the observed partial endosomal loss of WASH/retromer complexes (Fig 5C–H). Given the recently reported heterogeneity of retromer complexes [20], it is possible that RAB21 modulates the sorting of a defined set of cargos. Indeed, VARP was recently identified as a retromer interacting protein and shown to be involved in regulating a subset of VPS35-dependent cargos. Since RAB21 KO did not impact CI-MPR or GLUT1 trafficking, the VARP-dependent cargo MCT1 was assessed. RAB21 KO notably affected MCT1 protein levels (Fig 6D and E). This defect is reminiscent of what was observed in VARP-depleted cells [20], thus indicating that RAB21 modulates a subset of retromer cargos.

Interestingly, MCT1 (SLC16A1) was present in both GFP-Trap and APEX2:RAB21 datasets. Since SLC3A2, Basigin (CD147), and SLC16A3 were also observed in both datasets (Datasets EV1 and EV2), this could indicate that their trafficking may be regulated by RAB21, similar to MCT1. The interaction between RAB21 and SLC3A2 (Fig 6F) was thus first validated. Confirming the proteomic data, FLAG:RAB21 efficiently immunoprecipitated HA:SLC3A2. Given the available reagents, only SLC3A2 and Basigin trafficking were subsequently investigated. Importantly, these two cargos represent “direct CIE cargos” [72], which are characterized by their rapid sorting into tubular endosomes in HeLa cells [73]. As a result

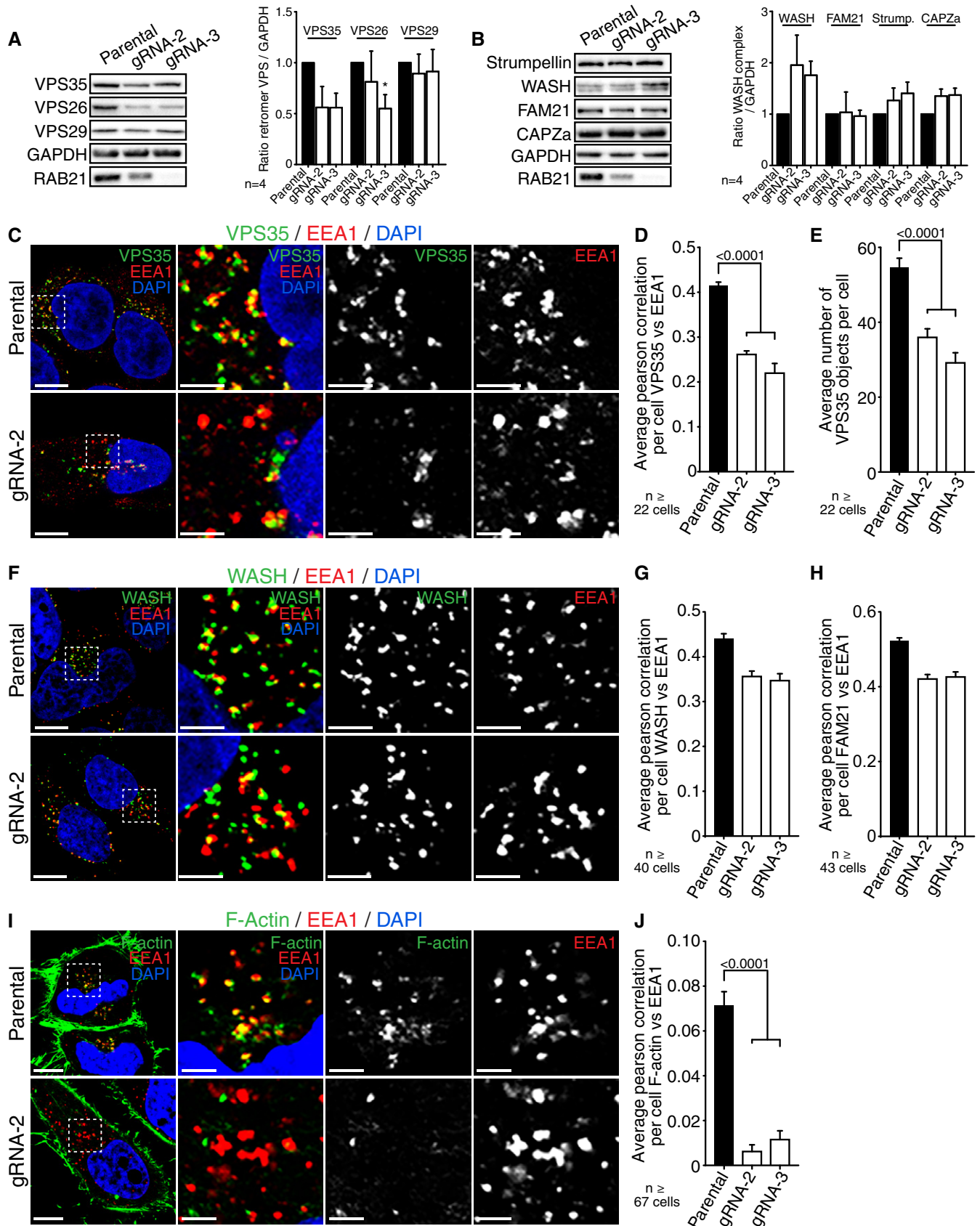


Figure 5.

**Figure 5. RAB21 modulates WASH and retromer endosomal recruitment and WASH activity.**

- A The stability of the retromer cargo sorting complex is affected in RAB21 KO cells. Immunoblot analysis of VPS35, VPS26, VPS29, GAPDH, and RAB21 in parental and the two RAB21 KO cell populations. Ratio of VPS35, VPS26, and VPS29 integrated densities to GAPDH of four independent experiments. \* $P < 0.05$ .
- B WASH complex proteins are not affected by RAB21 deletion. Immunoblot of Strumpellin, WASH, FAM21, CAPZ $\alpha$ , GAPDH, and RAB21. Ratio of WASH, FAM21, Strumpellin, and CAPZ $\alpha$  integrated densities to GAPDH of four independent experiments.
- C–E RAB21 knockout decreases VPS35 localization at endosomes. (C) Immunofluorescence of endogenous VPS35 and EEA1 in RAB21-depleted cells. Boxed region is magnified, and single-channel images are depicted. (D) Pearson's correlation per cell between VPS35 and EEA1,  $n = 3$  independent experiments. (E) Average number of VPS35 puncta per cell,  $n = 3$  independent experiments.
- F–H RAB21 loss impairs endosomal recruitment of the WASH complex. (F) Immunofluorescence of endogenous WASH and EEA1 in RAB21-depleted cells. Boxed region is magnified, and single-channel images are depicted. (G) Pearson's correlation per cell between VPS35 and EEA1 and (H) FAM21 and EEA1,  $n = 2$  independent experiments.
- I, J RAB21 knockout reduces endosomal F-actin levels. (I) Immunofluorescence of endogenous F-actin using Alexa 488-conjugated phalloidin and EEA1 in RAB21-depleted cells. Boxed region is magnified, and single-channel images are depicted. (J) Pearson's correlation per cell between internal F-actin and EEA1,  $n = 3$  independent experiments.

Data information: In (C, F, I), scale bars represent 10  $\mu\text{m}$  or 2.5  $\mu\text{m}$  in enlarged views. Statistical tests used are as follows: (A and B) one-sample  $t$ -tests, (D) unpaired  $t$ -tests, (E and J) Mann–Whitney tests. All error bars are SEM. Number of cells presented on each graph represents the total number of cells analyzed for all repeats.

of this feature, their tubular endosomal localization was monitored through a well-defined antibody uptake assay [74]. As expected, SLC3A2 and Basigin both localized to endosomal tubules in control cells (Fig 6G and H). Conversely, in RAB21 KO cells, both failed to reach tubular endosomes and were observed in a vesicular pattern (Fig 6G and H). Importantly, SLC3A2 presence on tubules was partially rescued by transient overexpression of FLAG:RAB21 WT (Fig EV5E). CD44, another well-defined “direct CIE cargo”, which was not observed in either the AP-MS or APEX2 datasets, was also followed in order to monitor whether RAB21 only affected interacting cargos or rather acted more generally in tubular endosome sorting events. CD44, similar to SLC3A2 and Basigin, failed to reach endosomal tubules in RAB21 KO cells (Fig 6G and H). These findings thus suggest a more general role of RAB21 in mediating fast endosomal sorting of “direct CIE cargos”.

Finally, to further corroborate that the loss of RAB21 affects the sorting of these cargos, steady-state SLC3A2 protein levels were followed, with the prediction that the latter would decrease due to lysosomal degradation, as observed for many retromer-dependent cargos [17]. In accordance with a sorting defect, an increased colocalization between SLC3A2 and late endosomes (RAB7) and lysosomes (LAMP1; Fig EV5F and G) was detected. Moreover, SLC3A2 total protein levels were decreased in RAB21 KO cells, as assessed by both FACS and immunoblotting (Fig EV5H and I). Altogether, these findings illustrate a new role for RAB21 in controlling endosomal sorting of direct clathrin-independent cargos.

### Both WASH and retromer complexes are required for SLC3A2 and Basigin sorting and for full RAB21 activity

To confirm that SLC3A2 and Basigin sorting to endocytic tubules require the WASH and retromer complexes, knockout HeLa cell populations for FAM21 (WASH), VPS29 (retromer), and VARP (retromer subcomplex; Fig 7A) were generated. Of note, both complexes were needed for full sorting of SLC3A2 and Basigin into endosomal tubules (Fig 7B and C). Although the effect was weaker compared to RAB21 (Fig 6H), there was a clear drop in the number of cells harboring SLC3A2- and Basigin-labeled tubules in FAM21, VPS29, and VARP knockout cells (Fig 7B and C). Importantly, SLC3A2 total protein levels were also downregulated in WASH and retromer knockout cells (Fig 7A and D). This latter finding is also in accordance with previous proteomic studies [17,75] and argues for

a common trafficking pathway essential for both SLC3A2 and Basigin sorting and requiring RAB21, WASH, and the retromer.

RAB21 interaction with the WASH/retromer complexes was independent of RAB21 GTP status (Fig 3C), thus suggesting that these complexes are unlikely to act as RAB21 effectors. Hence, it is possible that the retromer may additionally regulate RAB21 activity, given its association, through VPS29, with VARP, a RAB21 GEF [20,32,76]. This would provide a potential feedforward, or amplifying loop, to ensure concomitant RAB21 activation and retromer/WASH recruitment at specific endosomal cargos. To assess this, we monitored RAB21 endosomal localization in VPS29 and VARP KO cells. Interestingly, colocalization between RAB21 and EEA1 or VPS26 (Fig 7E–G) decreased in KO cells. Overall, these colocalization studies suggest that the retromer also regulates RAB21 functions, most likely through its interaction with VARP.

## Discussion

Defining a global picture of RAB GTPase interactors/neighbors has been hampered by inherent limitations related to the techniques used. Through the use and comparison of AP-MS and APEX2 proximity labeling, the present data show that APEX2:RAB proximity labeling was efficient at identifying RAB interacting/neighbor proteins ranging from GEFs, GAPs, effectors, and protein complexes. While important novel interactions were uncovered through the AP-MS technique, the APEX2 approach outperformed the former in terms of specificity and coverage. In addition, a new link between RAB21 and the WASH and retromer complexes was established from analysis of the proteomic datasets. As such, RAB21 was found to be required for complete recruitment of the WASH and retromer complexes to endosomes and for WASH-mediated actin polymerization. Moreover, RAB21 deletion compromised the trafficking of specific clathrin-independent cargos. This impairment was also observed in retromer or WASH complex-deleted cells. In light of the above, it is proposed that RAB21 and the retromer/WASH complexes operate in a feedforward loop to ensure their respective appropriate endosomal recruitment in order to mediate efficient cargo sorting (Fig 8).

By comparing the neighboring proteomes of three early endosomal RABs, a strong overlap between the latter was observed, in addition to specific enriched neighbors for each of these RABs, in

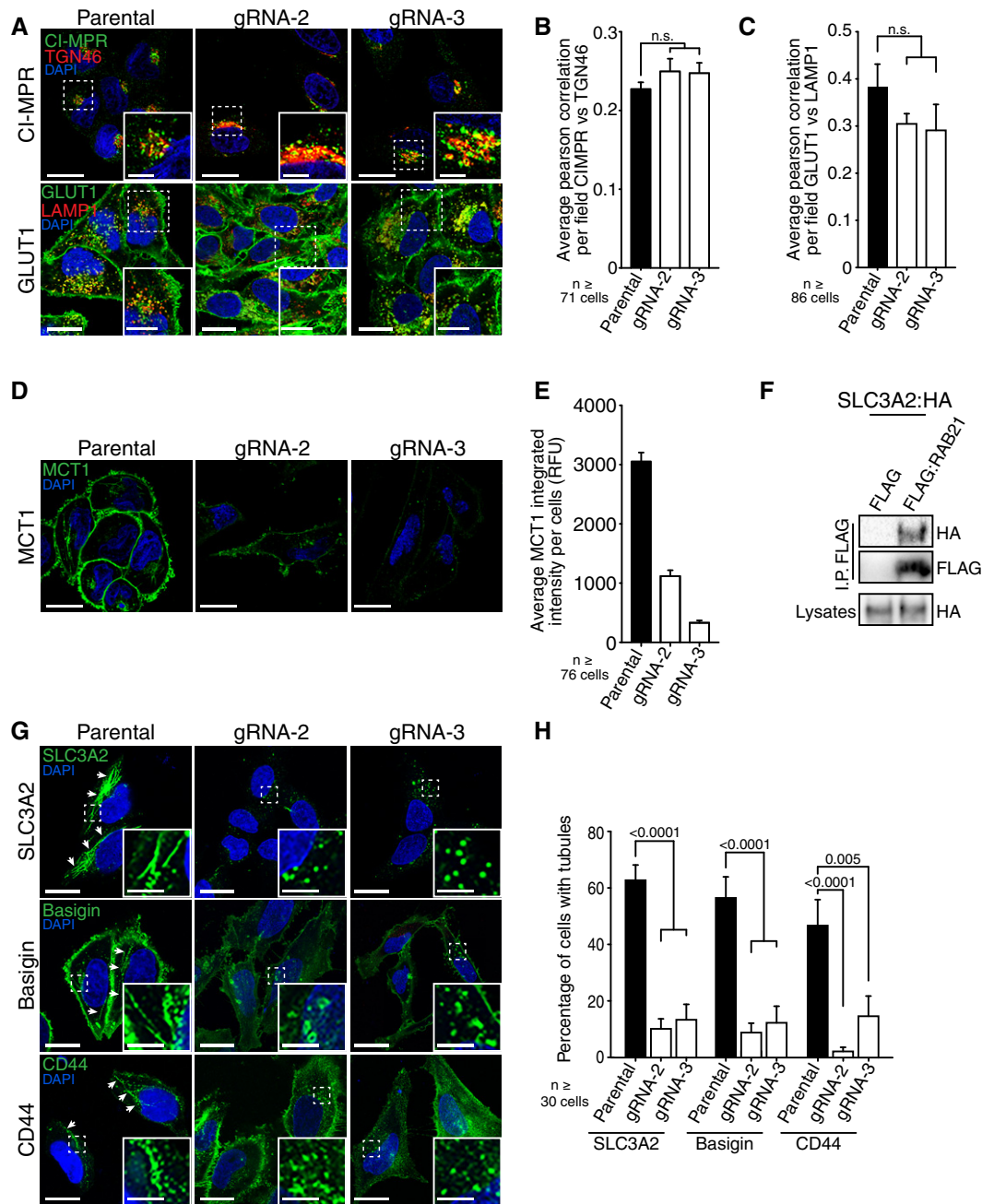


**Figure 6. RAB21 is required for endosomal sorting of specific cargo types.**

A–C RAB21 is not required for CI-MPR or GLUT1 trafficking. (A) Immunofluorescence of endogenous CI-MPR and TGN46 or GLUT1 with LAMP1 in RAB21 knockout cells. Boxed region is magnified. (B) Pearson's correlation per cell between CI-MPR and TGN46 or (C) GLUT1 and LAMP1,  $n = 3$  independent experiments.

D, E MCT1 trafficking requires RAB21. (D) Immunofluorescence of endogenous MCT1 in wild-type or RAB21-depleted cells. (E) Integrated MCT1 intensity per cell (in relative fluorescence unit),  $n = 2$  independent experiments.

F RAB21 interacts with SLC3A2. FLAG immunoprecipitation of FLAG:RAB21 and immunoblot of co-expressed SLC3A2:HA. Lysates correspond to 5% input,  $n = 3$  independent experiments.

G, H RAB21 is required for appropriate SLC3A2, Basigin, and CD44 trafficking. (G) Antibody uptake assays in parental or knockout RAB21 cells. Cells were stained with an Alexa 488-conjugated anti-mouse antibody. Arrowheads point to endosomal tubules. Note that non-internalized antibodies were removed by an acid wash, which was not fully efficient for CD147 and CD44, explaining plasma membrane labeling. (H) Percentage of cells with tubules in parental or RAB21 knockout cells,  $n = 3$  independent experiments.

Data information: In (A), scale bars represent 20  $\mu\text{m}$  or 5  $\mu\text{m}$  in enlarged views for CI-MPR, while they represent 10  $\mu\text{m}$  in enlarged views for GLUT1. (D and G) Scale bars represent 20  $\mu\text{m}$  or 5  $\mu\text{m}$  in enlarged views. Statistical tests used are as follows: (B) unpaired  $t$ -tests and (C and H) Mann–Whitney tests. All error bars are SEM. Number of cells presented on each graph represents the total number of cells analyzed for all repeats.

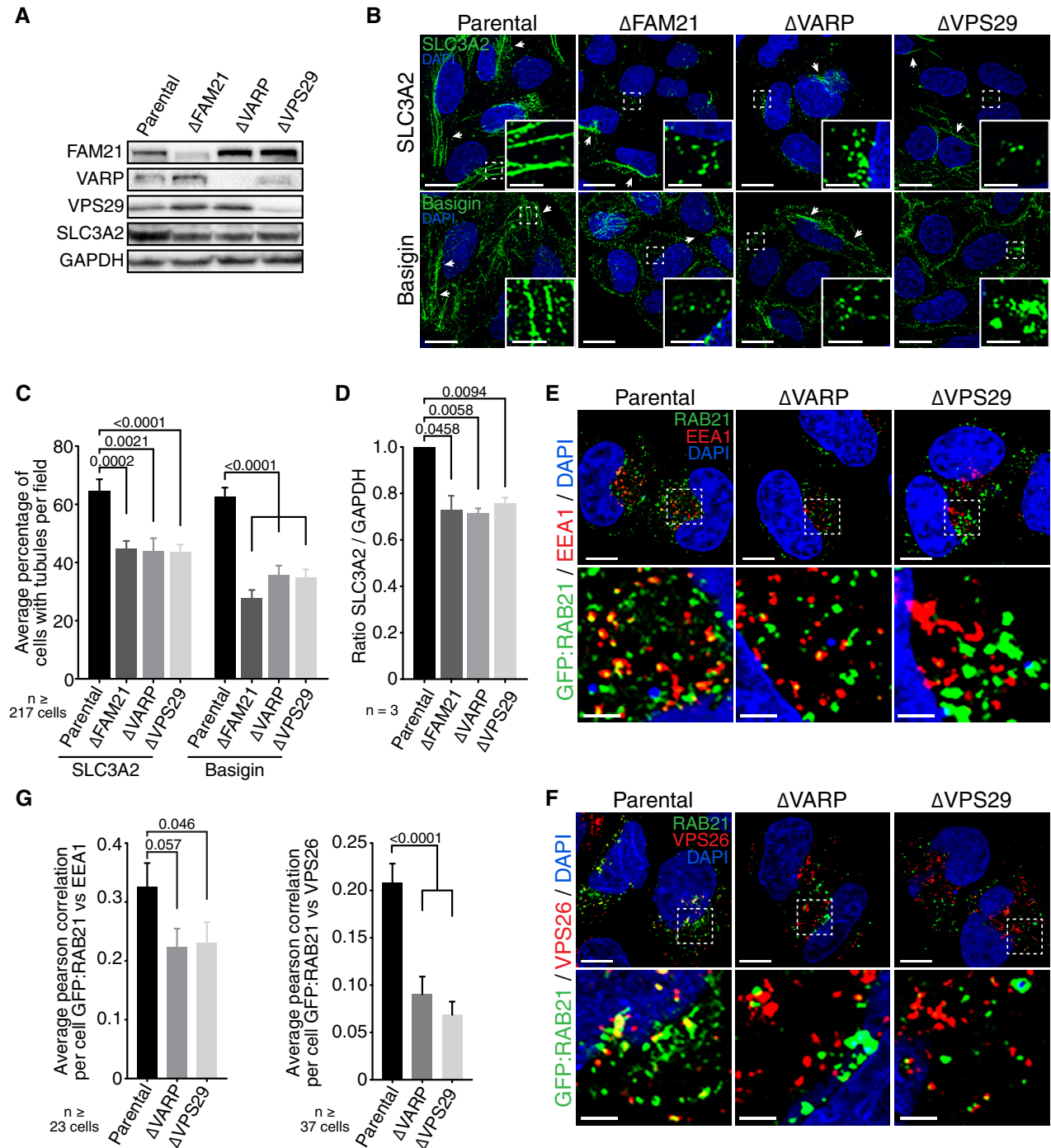


**Figure 7. WASH and retromer complexes are required for SLC3A2 and Basigin sorting, and for full RAB21 activation and endosomal localization.**

**A** Validation of WASH and retromer knockouts and SLC3A2 protein levels. Immunoblots of parental or FAM21, VARP, and VPS29 knockout cell populations.  
**B** Antibody-uptake assays in parental or knockout FAM21, VARP, and VPS29 cells. Cells were stained with an Alexa 488-conjugated anti-mouse antibody. Arrowheads point to endosomal tubules.  
**C** Percentage of cells with tubules in parental or in various knockout cells;  $n = 3$  independent experiments.  
**D** Ratio of SLC3A2 integrated densities to GAPDH;  $n = 3$  independent experiments.  
**E–G** Retromer is required for endosomal localization of RAB21. Immunofluorescence of transiently expressed GFP:RAB21 with endogenous (E) EEA1 or (F) VPS26 in parental or VARP- and VPS29-deleted cells. Boxed region is magnified underneath. (G) Pearson's correlation per cell between GFP:RAB21 and EEA1 or VPS26;  $n = 3$  independent experiments.

Data information: (B) Scale bars represent 20  $\mu\text{m}$ , (E and F) scale bars represent 10  $\mu\text{m}$  or 2.5  $\mu\text{m}$  in enlarged views. Statistical tests used are as follows: (C) unpaired  $t$ -tests, (D) one-sample  $t$ -tests, (G) Mann–Whitney tests. All error bars are SEM. Number of cells presented on each graph represents the total number of cells analyzed for all repeats.

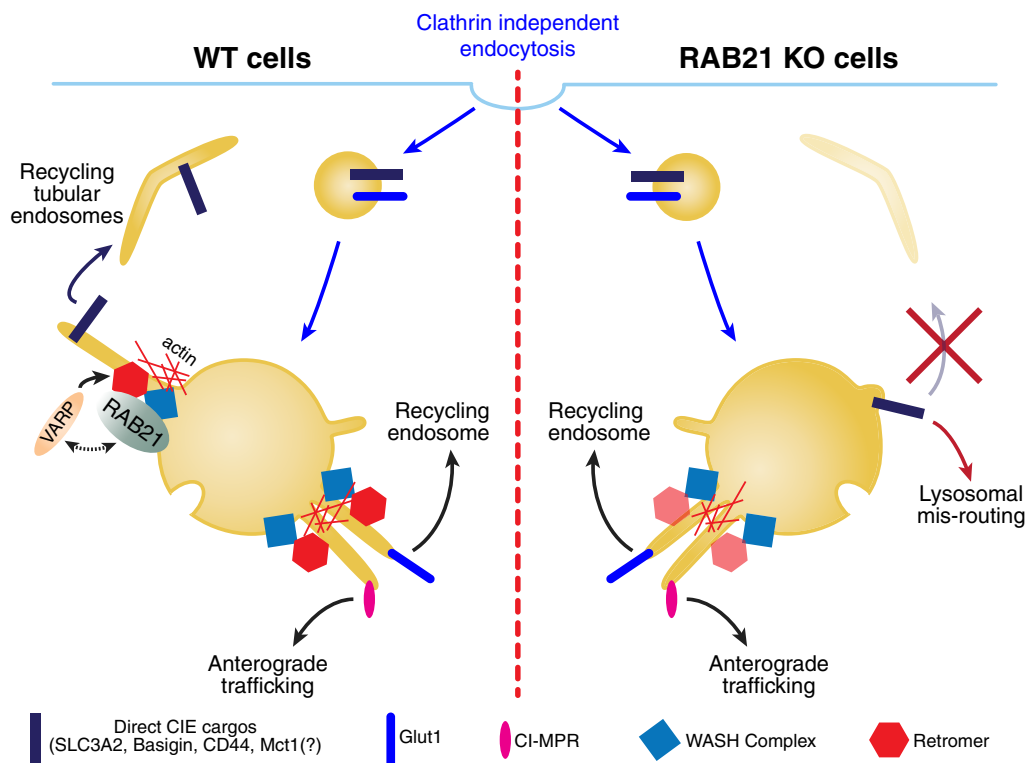


**Figure 8. Model of RAB21-mediated WASH/retromer cargo sorting.**

RAB21 is required for endosomal sorting of direct clathrin-independent cargos. RAB21 associates with WASH/retromer subcomplexes at endosomes. RAB21 could either (i) recruit WASH/retromer or (ii) be recruited by WASH/retromer or (iii) be part of a positive feedback loop that would allow WASH/retromer and RAB21 recruitment at endosomes. Endosomal RAB21 would be required for WASH-mediated F-actin polymerization. Although the data do not directly demonstrate a direct link between F-actin generation and cargo sorting, we propose that RAB21-dependent F-actin generation would be required for sorting of a CIE cargo subclass (MCT1, SLC3A2, Basigin, and CD44), while it would not be required for other cargos (CI-MPR or Glut1). In RAB21 knockout cells, decreased WASH/retromer endosomal localization is observed, which results in reduced endosomal F-actin and direct CIE cargo misrouting. This ultimately leads to the lysosomal degradation of these misrouted cargos (demonstrated for SLC3A2). Dotted line between VARP and RAB21 indicates that their coregulation with the retromer is speculative.

accordance with the concept of RAB microdomains [50,51]. These observations support the use of APEX2 as an efficient tool to identify RAB regulators/ effectors. One caveat however with APEX2 is that it does not discriminate between direct and indirect interactors, nor with bystander proteins. In general, proximity labeling often leads to the identification of a large quantity of proteins [49]. Indeed, there are a large number of statistically enriched proteins for all RABs, thus rendering their follow-up study prioritization difficult. Over 1,375 significant proteins were identified herein when combining four RABs. While they most probably not all represent direct interactors or direct RAB/protein complexes, the present data indicate that they reflect the protein environment associated with each RAB and that mining through these neighbors will likely be helpful for generating new hypotheses on RAB functions. However, because of the large number of identified proteins, it will be important to combine multiple approaches or datasets to help in establishing priorities. Here, the combination of GFP-Trap and APEX2 led us to identify a novel link between RAB21 and sorting of a subset of clathrin-independent cargos.

Given the vast amount of proteins recovered by APEX2:RAB, it is important to use appropriate controls to identify biologically relevant candidates. In our hands, normalization to APEX2 and the

direct comparison of related RABs yielded more valuable information than an ectopically endosomal-enriched probe. Moreover, when using a previously published APEX2:2xFYVE dataset [58], we observed that certain RAB interactors would have been filtered out, since they are also associated with PtdIns(3)P binding proteins (i.e., EEA1 [77]). Another approach that could define proteins more directly associated with RABs would be to use anti-biotin immunoprecipitation of trypsin-digested APEX2:RAB lysates in order to directly map biotinylated peptides [67]. Comparing the latter over a general streptavidin enrichment would in principle allow mapping of more direct interactions, as recently shown [78], and would most probably significantly reduce the number of identified proteins. Finally, we believe that expanding the repertoire of APEX2:RAB to each cell compartment will help toward identifying specific neighbors as already performed for phosphatases [49], and as observed herein when comparing APEX2:RAB7 to the three early endosomal RABs (Fig 2).

Since RAB21 proximity labeling enriched WASH and retromer complex members, the functional role between RAB21 and the WASH/retromer complexes was further investigated. Importantly, results from the co-immunoprecipitation and pull-down experiments showed that RAB21 interacts with multiple endogenous WASH and

retromer subunits. These findings strongly argue in favor of RAB21 binding to the WASH and retromer complexes. The fact that FAM21, Strumpellin, and CAPZ $\alpha$  were observed in pull-down studies further suggests that RAB21 directly interacts with the full WASH complex [79]. Nevertheless, the data do not allow to firmly conclude on this latter aspect and more defined structure–function studies will be required to map the WASH interaction site, as is also the case for VPS35 pull-down. It will be furthermore important in future studies to define which WASH- or retromer-specific subunit (s) is/are bound by RAB21 and to map the binding domains. Finally, congruent with our co-immunoprecipitation and pull-down results, RAB21 depletion partially impaired endosomal recruitment of the WASH and retromer complexes and also led to a decrease in endosomal F-actin and cargo trafficking impairments (Fig 8).

Given the observed role of RAB21 for WASH/retromer functions, one could have expected broader defects in RAB21 KO cells. No endosomal collapse, as observed in WASH or FAM21-depleted cells [80], or ectopic endosomal tubulation was observed in RAB21-deficient cells [19,28]. This is probably due to the fact that the WASH and retromer complexes are recruited at endosomes through multiple pathways. Both SNX3 and RAB7 have been shown to mediate endosomal retromer recruitment [13,14,81], while FAM21 binding to VPS35 has been found to be an important determinant of WASH endosomal recruitment [19,25,82]. However, recent studies have found that WASH can be recruited to endosomes independently of VPS35 [33,83]. Since only a partial reduction in retromer/WASH endosomal association was observed herein in RAB21 KO cells, a model in which RAB21 would be required for endosomal recruitment of a specific (or several) WASH/retromer complex(es) involved in the sorting of a subset of cargos is more in accordance with the observed data. This latter view is in agreement with newer models indicating heterogeneity in retromer sorting decisions and complexes [20,22,23]. Hence, while necessitating further confirmation, an appealing hypothesis would be that RAB21 could act in addition to RAB7 and SNX3, and directly recruit the WASH and retromer complexes to specific cargos. Another interesting possibility would be that RAB21 could function with either SNX3 or RAB7 in a co-incidence detection mechanism in order to recruit WASH/retromer complexes at endosomes, again to a subset of cargos. In this model, RAB21 would specify the type of WASH/retromer subcomplexes involved.

Another important aspect of this study is the decrease in detectable endosomal F-actin observed in RAB21-depleted cells. The exact mechanism by which RAB21 regulates WASH actin generation is unclear, given that WASH endosomal localization was only mildly affected in RAB21 KO cells. To draw an analogy with the WAVE complex [84,85], one could speculate that the WASH complex also requires the action of multiple inputs to drive full activation and actin polymerization. Ubiquitination was shown to regulate WASH activity [70], and it is conceivable that RAB21 could modulate this process, given its proximity to USP7 (Fig EV4B). Alternatively, it is also possible that RAB21 could modulate endosomal F-actin independently of WASH, through recruitment of another RAB21 interacting protein. Although outside the scope of this study, it would be interesting to test whether RAB21 can modulate WASH activation directly or indirectly. In keeping with the role of RAB21 in the endosomal tubule sorting of SLC3A2 and Basigin, it is worth noting that F-actin was shown to be required for formation and sorting of

“direct CIE cargos” [86]. This may also explain why RAB21 was also required for CD44 sorting, even though it did not interact with CD44. Given our findings that RAB21 and the WASH/retromer complexes are required for “direct CIE cargos” sorting, it could be suggested that these sorting events require F-actin generation, most probably for enrichment of cargos in tubules as previously reported for  $\beta$ 2AR [30] or for the formation of the tubules. Since loss of RAB21 had a stronger effect on CIE cargo tubule sorting, it is also possible that RAB21 plays a structural role by recruiting other effectors involved in the generation of these tubules, as also observed for RAB22 and RAB35 [74,87].

Of the various cargos tested herein, only “direct CIE cargos” were strongly impaired along with MCT1, a recently identified VARP-dependent cargo [20]. Our data thus suggest that MCT1 might also represent a “direct CIE cargo”, a possibility worth testing. The requirement of RAB21 for MCT1 trafficking also further strengthens our working model in which RAB21 would be involved in recruiting specific WASH/retromer subcomplexes to direct endosome-to-plasma membrane cargo trafficking. These “specific” WASH/retromer subcomplexes would most probably include VARP while excluding TBC1D5 since VARP and TBC1D5 binding sites on VPS29 share the same interface and are thought to be mutually exclusive [19,32].

Another noteworthy finding from the current proteomic experiments was the specific presence of TBC1D23 in APEX2:RAB21 proximity labeling. Recent work has identified TBC1D23 as a bridge factor for endosomal-to-Golgi carriers [88]. In this study, TBC1D23 was shown to interact directly and simultaneously with either golgin-97 or golgin-245 and the WASH complex [88]. Importantly, TBC1D23, like the WASH complex, was required for TGN46 endosome-to-Golgi trafficking. It was also proposed that another factor could act together with FAM21 to increase the specificity of captured vesicles. Given our demonstrated interaction with the WASH complex and the presence of TBC1D23 in APEX2:RAB21, RAB21 could represent such a factor. However, we did not observe strong defects in either CI-MPR or TGN46 trafficking in RAB21 KO cells. While this latter observation argues against RAB21 playing a predominant role in this retrieval pathway, RAB21 could nonetheless still be involved in specifying vesicle subtypes that are different from CI-MPR- and TGN46-containing vesicles.

The WASH complex has also been recently associated with the retriever complex [33]. This VPS29-, C16orf62-, DSCR3-containing core complex, akin to the VPS35, VPS29 and VPS26 cargo retromer complex, functions with SNX17 to regulate the sorting of a large array of cargos. Importantly, proteomic analyses showed distinct and overlapping cargos with the retromer [33]. In the present study, C16orf62 was enriched in RAB21 proximity labeling whereas DSCR3 and SNX17 were not, while CCC complex members were observed with variable enrichment ratios (Dataset EV2). Hence, RAB21 could possibly be involved in regulating WASH and retriever complex formation and/or sorting. Our experimental validation of RAB21 was specifically focused on the shared roles of RAB21 with the WASH and retromer complexes. In the present instance, retromer-versus retriever-specific functions were not discriminated due to the use of a VPS29 knockout. Given the role of VPS29 with the retriever complex, certain observed phenotypes could have been caused by a loss of retriever activity. However, our demonstration that RAB21 functionally interacts with the WASH and retromer complexes is

robust given that all knockouts shared similar SLC3A2 and Basigin trafficking impairments. Significantly, loss of VARP function, which is independent of retriever activity and associated with the retromer, shared the same RAB21 phenotypes on cargos. Importantly, endosomal c16orf62 localization was not decreased by RAB21 deletion, but rather increased (Fig EV5J), thus suggesting that RAB21 could potentially modulate the balance between retromer and retriever complex association with endosomes, possibly through RAB21 interaction with the WASH complex or through VARP. Again, this represents an exciting new possibility which will require further validation.

In summary, through the use of unbiased proteomics, the present study allowed uncovering novel functional roles for RAB21 in direct clathrin-independent sorting events. Results also demonstrate the robustness and ease of APEX2-mediated proximity labeling and its applicability to efficiently identify novel RAB-specific functions. This approach may be further extended to temporally generate dynamic findings on RAB GTPases under various cellular stimulations, thereby leading to a better definition of RAB GTPase regulation and their association with their respective effectors.

## Materials and Methods

### Cell culture

HCT116 and HeLa Flp-in/T-REx cells and HeLaM cells (gift from T. Yoshimori) were grown in Dulbecco's modified Eagle's medium (DMEM) supplemented with 10% fetal bovine serum (Wisent) at 37°C and 5% CO<sub>2</sub>. FT cells were maintained under selection with 100 µg/ml Zeocin and 5 µg/ml blasticidin. FT control cells are the non-recombined parental cells and were used as control in all SILAC experiments, as performed previously [43,89]. All cells were routinely screened for mycoplasma contaminations, and experiments were excluded if contamination was observed. To recombine the various GFP:RAB21 variants, APEX2:RAB4a, 5a, 7a, and APEX2:RAB21 in cells, FT cells were transfected with jetPRIME (Polyplus), according to manufacturer's instruction. A RAB/pOG44 DNA ratio of 1–10 was used, such that 0.1 µg of pGLAP:RAB was cotransfected along with 0.9 µg of pOG44 (Thermo Fisher) in individual wells of a 6-well plate. Twenty-four hours following transfection, recombinant cells were selected with 5 µg/ml blasticidin and 100 µg/ml hygromycin (150 µg/ml for HeLa cells). Following selection, cells were pooled and a polyclonal population was expanded and used for all subsequent experiments. RAB21, RAB4, RAB5, RAB7 expression was achieved through addition of doxycycline at 10 ng/ml final concentration for 24 h prior to all experiments.

For SILAC experiments, FT cells were maintained in light DMEM (R0K0: Arg0, Sigma, A5006; Lys0, Sigma, L5501), while GFP:RAB21 variants were grown in medium (R6K4: Arg6, Cambridge Isotope Lab (CIL), CNM-2265; Lys4, CIL, DLM-2640) or heavy (R10K8: Arg10, CIL, CNLM-539; Lys8, CIL, CNLM-291) DMEM depleted of arginine and lysine (Life Technologies A14431-01), and supplemented with 10% dialyzed fetal bovine serum (FBS; Invitrogen, 26400-044), called SILAC medium. Cells were passaged 5 times to ensure proper incorporation of all heavy amino acids, prior to SILAC experiments.

### Generation of DNA constructs

GFP:RAB21 variants were PCR-amplified from previously published pCDNA3 variants [42] and ligated using the In-Fusion HD kit (Clontech) into a PCR-amplified modified pGLAP1 vector [43] where GFP was placed N-terminally to the fusion protein. APEX2:RAB21-WT was generated by PCR amplification of RAB21-WT from pCDNA3-GFP:RAB21-WT and subcloned by In-Fusion HD in pGLAP1-APEX2. This vector is a modified version of N-terminal pGLAP1 vector, where the GFP was replaced with Myc:APEX2 [90]. APEX2:RAB4a, APEX2:RAB5a, and APEX2:RAB7a were generated by PCR amplification of RAB4a, 5a, and 7a from HeLa cell cDNA. cDNA was generated with the SuperScript III First-Strand Synthesis kit (Thermo Fisher Scientific) and PCR performed with the Phusion enzyme (New England Biolabs). PCR fragments were cloned by In-Fusion HD in pGLAP1-APEX2. All clones were subsequently sequenced and validated.

### Immunoprecipitations, mass spectrometry, pull-downs, and immunoblots

A total of  $8 \times 10^6$  cells were plated in 150-mm plates and grown for 2 days in appropriate SILAC medium, followed by a 24-h doxycycline induction (10 ng/ml). Cell lysis was performed in 2.2 ml of CoIP buffer (25 mM Tris-HCl pH 7.4, 1 mM EDTA, 0.1 mM EGTA, 15 mM MgCl<sub>2</sub>, 150 mM NaCl, 2 mM Na<sub>3</sub>VO<sub>4</sub>, 10% glycerol, 1% IGEPAL CA-630, 2× protease inhibitors) per plate, and cells were incubated for 20 min on ice. Lysates were cleared by centrifugation at 16,000 g for 10 min at 4°C. Cell lysates were quantified through a BSA assay (Pierce), and equal amounts were immunoprecipitated in individual tubes with 20 µl of GFP-Trap beads (ChromoTek) and incubated on a rotator for 2.5 h at 4°C. Beads were washed twice with full lysis buffer and twice again with lysis buffer lacking IGEPAL CA-630. This was followed by five washes of 20 mM NH<sub>4</sub>HCO<sub>3</sub>. Following these washes, GFP-Trap beads from three independent immunoprecipitations (light, medium, and heavy) were mixed equally and processed for on-beads digestion and mass spectrometry analysis following these steps. Proteins were reduced 30 min with 10 mM DTT and alkylated 1 h with 15 mM iodoacetamide. After iodoacetamide quenching with 15 mM DTT, proteins were digested overnight with 1 µg trypsin. Digestion was stopped by acidification with 1% formic acid, supernatant was collected, and residual peptides were eluted with 60% acetonitrile and 0.1% formic acid. Samples were then dried, resuspended in 0.1% TFA solution, and desalted on a Zip Tip. Trypsin-digested peptides were loaded and separated using an Ultimate 3000 nanoLC (Thermo Fisher Scientific Inc). Ten microliters of the sample (2 µg) resuspended in 1% (v/v) formic acid was loaded onto a trap column (Acclaim PepMap100 C18 column, 0.3 mm id × 5 mm, Dionex Corporation, Sunnyvale, CA), and the peptides were separated by a PepMap C18 nanocolumn (75 µm × 50 cm, Dionex Corporation) with a linear gradient of 5–35% solvent B (90% acetonitrile with 0.1% formic acid) over a 4 h gradient with a constant flow of 200 nl/min. Acquisition of the full-scan MS survey spectra (m/z 350–1,600) in profile mode was performed in a Q Exactive Orbitrap (Thermo Fisher Scientific Inc) at a resolution of 70,000 using 1,000,000 ions. All unassigned charge states as well as singly, 7 and 8 charged species for the precursor ions were rejected. To improve the mass accuracy of

survey scans, the lock mass option was enabled. Data acquisition was performed using Xcalibur version 2.2 SP1.48.

GST and GST:RAB21 were purified exactly as described in Ref. [91] for GST:APPL1, and pull-downs were carried out with equal amounts of GST or GST:RAB21. Pull-downs were performed as follows.  $3.5 \times 10^6$  HeLa cells were plated in 100 mm plates, and 24 h later, cells were lysed for 20 min on ice with 1 ml of MLB modified buffer (25 mM HEPES, 150 mM NaCl, 1% IGEPAL CA-630, 10% glycerol, 20 mM  $MgCl_2$ , 1 mM sodium orthovanadate, 100  $\mu$ M EGTA and 100  $\mu$ M GTP) supplemented with protease inhibitors. Lysates were cleared by centrifugation at 16,000 g for 10 min at 4°C. In the meantime, GST and GST:RAB21 sepharose beads were washed three times in MLB modified buffer minus IGEPAL CA-630 and incubated for 20 min at 4°C with rotation in modified MLB buffer without IGEPAL CA-630. Beads were then washed three times with MLB modified buffer and incubated with 900  $\mu$ l of lysates for 1 h at 4°C with rotation. Finally, lysates were discarded and beads were washed three times with MLB modified buffer containing 0.2% IGEPAL CA-630. Media were removed, and 30  $\mu$ l of 2 $\times$  SDS loading buffer was added to each sample.

For immunoblots, protein extracts were separated on 4–20% TGX precast gels (Bio-Rad) and transferred on PVDF (Millipore) membranes. Antibodies used for immunoblotting were anti-GFP (1:500, Roche #11814460001), anti-RAB21 (1:1,000, Sigma #R4405 or 1:1,000, Invitrogen #PA5-34404), anti-RAB4 (1:1,000, Cell Signaling #2167), anti-RAB5 (1:1,000, Cell Signaling #3547), anti-RAB7 (1:1,000, Cell Signaling #9367), anti-GAPDH-HRP (1:1,000, Cell Signaling #8884), anti-Myc (1:1,000, Cell Signaling #2278), anti-HA (1:1,000, Cell Signaling #3724), anti-SLC3A2 (1:800, Cell Signaling #13180), anti-Strumpellin (1:500, Santa Cruz #377146), anti-VPS35 (1:500, Santa Cruz #374372), anti-VPS26 (1:500, Santa Cruz #390304), anti-VPS29 (1:500, Santa Cruz #398874), anti-FAM21 and anti-WASH (1:10,000, gift from D. Billadeau), anti-CAPZ $\alpha$  (1:500, Santa Cruz #374302), anti-APPL1 (1:1,000, Cell Signaling #3858), anti-VARP (1:500, Bethyl Laboratories #A302-997A), anti-tubulin (1:2,500, Sigma #T9026), streptavidin-HRP (1:1,000, Thermo Fisher #N100), and anti-rabbit and mouse HRP (1:10,000, Jackson Laboratories #115-035-144 and #115-035-146, respectively). Luminata Forte (Millipore) or Clarity Max chemiluminescent substrates were used, and membranes imaged on a Bio-Rad Chemidoc XR station.

## APEX2

A total of  $8 \times 10^6$  HeLa cells were plated in 150 mm plates and induced 24 h later with 10 ng/ml doxycycline for 24 h. Freshly prepared biotin–phenol was added to full DMEM to yield a final concentration of 500  $\mu$ M. After renewal of the culture medium, cells were incubated in DMEM—biotin–phenol—for 30 min at 37°C. Biotinylation was achieved by adding freshly prepared  $H_2O_2$  at a final concentration of 2 mM for exactly 1 min. Reactions were halted by removing the media, transferring the cells on ice, and performing five washes, each wash for 1 min, in freshly prepared quencher buffer [1 $\times$  PBS containing 10 mM sodium azide, 10 mM sodium ascorbate, and 5 mM Trolox (Sigma)]. Cells were then processed as detailed for co-immunoprecipitations (CoIPs), with the following changes. Protein lysates were incubated with 20  $\mu$ l of streptavidin agarose beads (GE Life Sciences) or 20  $\mu$ l of biotin antibody agarose beads (ImmuneChem Pharmaceuticals) for 2.5 h at

4°C on a rotating wheel. Beads were then washed twice in CoIP buffer containing 1% IGEPAL CA-630, twice in CoIP buffer minus IGEPAL CA-630 and five times with 20 mM  $NH_4HCO_3$ . Lysates were analyzed by immunoblots, and affinity-purified biotinylated proteins were processed for Western blots or for on-beads digestion and mass spectrometry analysis as described above.

## Experimental design and statistics

For SILAC experiments, two biological repeats were performed in each cell line for each RAB21 variant, yielding a total of four independent samples per variant analyzed when HeLa and HCT116 data were combined. For APEX2 experiments, results were obtained from three independent biological repeats. Controls (FT) were included in all SILAC mass spectrometry experiments. Hence, a total of six independent FT controls were used in SILAC experiments and three APEX2-alone controls in APEX2 experiments. Statistical analyses of objects count or colocalization results were performed using Prism 7 software. Endosomal tubules were assessed manually. Briefly, the number of cells per field was established using DAPI staining, and cells harboring  $\geq 2$  tubules were counted as positive. An average per field was established, and multiple fields of at least two independent experiments were pooled and analyzed using Prism software. For all analysis, the average number of object puncta or tubules or the average Pearson correlation per cell was tested for normality using a D'Agostino–Pearson omnibus normality test. Samples that showed normal distribution were analyzed through unpaired *t*-tests, while samples showing a non-normal distribution were compared through nonparametric Mann–Whitney tests to assess the significance between the various conditions. All graphs display SEMs to assess variations within each group. For Western blot quantifications, bands were quantified on the Image Lab software (Bio-Rad) and normalized to parental cells. One-sample *t*-tests were performed for statistical analyses.

## Mass spectrometry hit selection and network generation

After analysis by nanoLC-MS/MS, peptides and proteins were identified by MaxQuant version 1.5.2.8 using UniProt (*Homo sapiens*, 16/07/2013, 88354 entries, Datasets EV1 and EV2). Trypsin/P was the set enzyme, with no cleavages on arginines or lysines preceding a proline, with a maximum of two miscleavages being allowed. Mass tolerance of 7 and 20 ppm was used for precursor and fragment ions, respectively. Fixed carbamidomethyl modification on cysteine and variable oxidation on methionine and N-terminal acetylation were settled. For reliable identification, all proteins needed to complete a false discovery rate (FDR) inferior to 1%: All proteins whose hits from the forward database were not 100-fold superior to hits from the reverse database were discarded. For SILAC conditions, the re-quantification option was selected. A minimum of two quantified peptides was settled for proteins to be considered. For a peptide, following its identification, MaxQuant used the median ratio to approximate a SILAC value for that particular peptide. Likewise, in order to establish a protein–SILAC ratio, MaxQuant used the median ratio of all identified peptides, a method shown to be appropriate for estimation of SILAC ratios [92]. To determine the RAB21 interactome from SILAC GFP-Trap experiments, only proteins with an intensity (RAB21-expressed condition)/intensity

(FT control condition) ratio  $> 2$  in both experimental repeats were considered as potential RAB21 interactors [43,89]. In the case of APEX2 affinity purification–mass spectrometry (AP-MS) experiments, the ProHits software suite [93] was used to compare all samples (APEX2, APEX2:RAB4a, APEX2:RAB5a, APEX2:RAB7a, APEX2:RAB21, and APEX2:2xFYVE (the raw MS data for APEX2:2x-FYVE were downloaded from the ProteomeXchange Consortium). First, SAINTexpress was run on the Crapome platform to establish high probability interactors. Default settings were used to compare user control, in this instance, APEX2 to each APEX2:RABs [52]. Only proteins with SAINT scores above 0.95 were selected. Thereafter, SAINT raw results were extracted and used to generate dot plots or cluster plots on a ProHits-viz platform. In order to account for experimental variations, all samples were normalized on ProHits-viz for dot plot representations. Once RAB21 potential interactors were identified, RAB21 protein interaction networks were generated on Cytoscape. Results were combined by cell lines (HeLa or HCT116), and once interaction networks were created, proteins were sorted based on their Genecard and UniProt subcellular localization data. Each color corresponds to a different localization. Cytoscape platform was used to generate biological Reactome process enrichments using Reactome plugging among specific generated networks. To compare differential protein enrichments depending on RAB21 status, SILAC RAB21-variant mean ratios were transformed in  $\log_2(x)$  and 0 was imputed to non-available data. Default settings from the Perseus software [94] were used to generate hierarchical clustered heat maps.

### Immunofluorescence, colocalization, and transferrin or antibody uptake

A total of 70,000 HeLa or HCT116 cells were plated on glass coverslips (#1.5) and grown for 24 h followed by GFP:RAB21 variant induction as performed above. Cells were then washed twice with  $1\times$  PBS and fixed for 15 min at room temperature in 4% paraformaldehyde in PBS or, depending on the antibody, in 100% methanol at  $-20^\circ\text{C}$  for 20 min. Cells were then washed three times with PBS for 5 min each, blocked, and permeabilized for 60 min at room temperature in PBS containing 5% goat serum and 0.3% Triton X-100. Cells were then incubated in primary antibodies overnight at  $4^\circ\text{C}$  in PBS containing 1% BSA and 0.3% Triton X-100. Primary antibodies were washed three times for 5 min in PBS at room temperature and incubated at room temperature for 1 h in secondary antibodies diluted in antibody dilution buffer. Following secondary antibody incubation, three 5-min washes in PBS at room temperature were performed and cells were mounted in DAPI-containing mounting media (Sigma) and subsequently imaged. Antibodies used were anti-EEA1 (1:100, Cell Signaling #3288; or 1:1,000 BD Biosciences #610456), anti-SLC3A2 (1:800, Cell Signaling #13180; or 1:400 Santa Cruz #376815), anti-transferrin receptor (1:100, Cell Signaling #13113), anti-RAB7 (1:250, Santa Cruz #376362), anti-LAMP1 (1:250, Santa Cruz #20011), anti-LC3B (1:100, Cell Signaling #3868), anti-APPL1 (1:100, Cell Signaling #3858), streptavidin–Alexa 647 (1:500, Thermo Fisher #S21374), anti-FAM21 or anti-WASH (1:1,000, gift from D. Billadeau), anti-VPS26 (1:100, Abcam #23892), anti-VPS35 (Santa Cruz, 1:100 #374372), anti-SNX1 (1:100, Abcam #ab995), phalloidin–Alexa 488 (1:1,000, Invitrogen #A12379), anti-CI-MPR (1:100, Bio-Rad #MCA2048T), anti-TGN46 (1:100, Novus Biological

#NBP1-49643SS), anti-Glut1 (1:500, Abcam #115730), anti-MCT1 (1:100, Genetex #GTX631643), and goat anti-mouse or rabbit Alexa 488 or 546 (1:250, Thermo Fisher #A11030, A11035, A11029, and A11034). DAPI was used to unbiasedly identify fields where images were acquired.

For transferrin uptake, cells were plated at a density of 40,000 cells on (#1.5) glass coverslips and grown for 24 h. Cells were serum-starved for 30 min in DMEM. Alexa 647-labeled transferrin was added at  $25\ \mu\text{g}/\text{ml}$  and allowed to bind to the receptor for 15 min on ice. Cells were washed with cold PBS and incubated in FBS-supplemented DMEM for 0–60 min at  $37^\circ\text{C}$ . Cells were washed in PBS and fixed with 4% PFA for 15 min at room temperature and mounted for imaging. SLC3A2 (clone MEM-108, Biolegend), Basigin (clone HIM6, Biolegend), and CD44 (clone BJ18, Biolegend) uptake assays were performed exactly as previously described [74].

Figures 1D, 4B, EV1C, EV4G, and EV5F were acquired on an Olympus FV1000 confocal microscope equipped with a  $60\times/1.42\text{NA}$  Plan Apo N objective at a  $1\times$  zoom (colocalization) or a  $40\times/1.3\text{NA}$  UPLANFLN objective (LC3 counts). Single Z-sections were acquired, and acquisition settings were set to avoid pixel saturation to ensure proper colocalization and intensity quantification. Images were adjusted similarly between conditions to accurately represent the raw data. Figures 3E, 5C, F, and I, 6A, D, and G, and 7B, E, and F, EV5A, D, and J were acquired on a ZEISS LSM880 equipped with a  $40\times/1.4\text{NA}$  Plan Apo objective at a  $1.6\times$  zoom. For colocalization experiments, single Z-sections were acquired and gain/offset settings were similarly adjusted between conditions. For some antibodies, offset was utilized in order to remove non-specific intracellular background signal and to facilitate endosomal localization visualization. For endosomal tubule imaging, three Z-sections were acquired at  $0.36\ \mu\text{m}$  each and maximum intensity projections were generated. These maximum intensity projections were used for data quantification and representation. Finally, only linear modifications of levels were performed on Photoshop CC2017. Cropping and resolution changes to 300 dpi were also performed on Photoshop for data presentation. Image colocalization was achieved with CellProfiler [95]. Briefly, GFP:RAB21 cells were identified manually or through a primary object identification module and the correlation coefficient (Pearson) was measured on original images using the measure correlation module. Number of object puncta per cells was also achieved using CellProfiler. For both colocalization and objects count, all measurements were exported to Prism for statistical analyses.

### Generation of knockout HeLa cells

RAB21 knockout HeLa cell populations were engineered using the CRISPR/Cas9 technique. Briefly, guide RNAs were selected based on Ref. [96]. Two independent gRNAs (gRNA-2 “AGTAAATTGGACCAATGCA” and gRNA-3 “CCACCTTGAACGAGTAGGCT”) were selected and cloned into pSPCas9(BB)-2A-Puro. A total of  $1 \times 10^6$  HeLa cells were plated in 100-mm dishes and transfected with individual plasmids. After 24 h, transfected cells were selected with  $1.5\ \mu\text{g}/\text{ml}$  puromycin for 5 days, with media renewed every 48 h. Selected cells were amplified and frozen at low passages. Deletion of the RAB21 gene was verified by PCR and sequencing. Briefly, genomic DNA isolated from each gRNA-selected cell population was isolated. Amplicons encompassing predicted cut sites were

amplified by PCR (using Phusion polymerase) and ligated into pBluescript using T4 DNA ligase. Individual bacterial clones were selected and sequenced, and the representation of the cutting events is depicted in Fig EV4E. All experiments performed on knockout cells were performed at low passages to avoid competition from potential non-targeted wild-type HeLa cells.

HeLa FAM21, VPS29, and VARP knockout cell populations were performed as in Ref. [97]. Briefly, three independent gRNAs cloned into the PX330A plasmid were cotransfected with the pEGFP-Puro plasmid (addgene #45561) at a ratio of 1:1:1:0.25. Transfections were performed as detailed above. Twenty-four hours after the transfections, cells were selected for 24 h with 2 µg/ml puromycin. Cells were amplified and used at low passages for all experiments. gRNA sequences for VPS29 and FAM21 have been published in Ref. [97], while gRNAs for VARP were AAGAGCCACTCACGTCCTCG, CAGCACGGCTACTGACTATG, and TAAATACGTGGGGACCATGG. Knockout efficiencies were monitored by Western blot.

### FACS analysis

A total of  $1 \times 10^6$  HeLa parental and gRNA KO 2 and 3 cells were trypsinized, collected, and washed with cold PBS. Cells were fixed 15 min with PFA 4% and permeabilized with methanol 90%, for 30 min. Cells were labeled (or not) with SLC3A2 rabbit antibody (dilution 1:800, Cell Signaling #13180) in PBS/BSA 0.5% incubation buffer for one hour. After two PBS washes, cells were incubated for 30 min in secondary Alexa Fluor 488 antibody (dilution 1:250) diluted in incubation buffer. For each condition, Alexa Fluor 488 signal intensity was measured with a BD LSR Fortessa cytometer. Acquisition was made using BD FACSDiva software, and graphics and analysis using Flowing software 2.5.1. Mean 488 intensity signal ratios from SLC3A2 labeled cells versus non-labeled cells were used to compare SLC3A2 expression levels between the different cell lines. Signal intensity distributions from each cell line were overlapped on the same frequency histogram. In order to optimize visualization, data were submitted to virtual gain, such that  $f(x) = 60x + 15,000$ , with  $x$  being the intensity signal. The displayed diagram (Fig EV5H) reflects one representative experiment from the three performed repeats and represents 10,000 counted cells per cell line.

### Data availability

The SILAC and APEX2 mass spectrometry proteomic data from this publication have been deposited to the ProteomeXchange Consortium via the PRIDE partner repository (<https://www.ebi.ac.uk/pride/archive/>) and assigned the dataset identifier PXD010950.

**Expanded View** for this article is available online.

### Acknowledgements

We thank M.L. Dubois and D. Lévesque for helpful technical assistance with mass spectrometry and SILAC experiments, V. Delcourt for help with Perseus, C. Lavoie for generously providing multiple antibodies, M. Catala for help with FACS analysis, D. Billadeau for kindly providing the FAM21 and WASH antibodies, and Amy Kiger for support in establishing tools for the current study. We also thank all members of the Jean laboratory for insightful

comments during the course of this study. We thank the proteomic platform at the Université de Sherbrooke for proteomic services and the Photonic microscopy platform for confocal use. Steve Jean and François-Michel Boisvert are members of the FRQS-Funded Centre de Recherche du CHUS. Steve Jean is a recipient of a Research Chair from the *Centre de recherche médicale de l'Université de Sherbrooke* (CRMUS). This research was supported by operating grants from the Cancer Research Society (CRS), the Natural Sciences and Engineering Research Council of Canada (NSERC), and the Canadian Institutes of Health Research (CIHR) and by junior faculty salary awards from Canadian Institutes of Health Research (CIHR) and Fonds de Recherche du Québec—Santé (FRQS) to S.J.

### Author contributions

TDO, AL, RL, ML, DJ, LL, and SJ performed experiments. CN quantified colocalization data. F-MB assisted and helped with all mass spectrometry analyses. FS provided multiple reagents and suggestions. SJ and TDO designed experiments. SJ supervised students and wrote the manuscript.

### Conflict of interest

The authors declare that they have no conflict of interest.

### References

1. Stenmark H (2009) Rab GTPases as coordinators of vesicle traffic. *Nat Rev Mol Cell Biol* 10: 513–525
2. Nicot A-S, Laporte J (2008) Endosomal phosphoinositides and human diseases. *Traffic* 9: 1240–1249
3. Amoasii L, Hnia K, Laporte J (2012) Myotubularin phosphoinositide phosphatases in human diseases. *Curr Top Microbiol Immunol* 362: 209–233
4. Santiago-Tirado FH, Bretscher A (2011) Membrane-trafficking sorting hubs: cooperation between PI4P and small GTPases at the trans-Golgi network. *Trends Cell Biol* 21: 515–525
5. Jean S, Kiger AA (2012) Coordination between Rab GTPase and phosphoinositide regulation and functions. *Nat Rev Mol Cell Biol* 13: 463–470
6. Rojas AM, Fuentes G, Rausell A, Valencia A (2012) Evolution: the ras protein superfamily: evolutionary tree and role of conserved amino acids. *J Cell Biol* 196: 189–201
7. Hutagalung AH, Novick PJ (2011) Role of Rab GTPases in membrane traffic and cell physiology. *Physiol Rev* 91: 119–149
8. Barr F, Lambright DG (2010) Rab GEFs and GAPs. *Curr Opin Cell Biol* 22: 461–470
9. Itoh T, Satoh M, Kanno E, Fukuda M (2006) Screening for target Rabs of TBC (Tre-2/Bub2/Cdc16) domain-containing proteins based on their Rab-binding activity. *Genes Cells* 11: 1023–1037
10. Barr F, Lambright DG (2010) Rab GEFs and GAPs. *Curr Opin Cell Biol* 22: 461–470
11. Barr FA (2013) Rab GTPases and membrane identity: causal or inconsequential? *J Cell Biol* 202: 191–199
12. Grosshans BL, Ortiz D, Novick P (2006) Rabs and their effectors: achieving specificity in membrane traffic. *Proc Natl Acad Sci USA* 103: 11821–11827
13. Rojas R, Van Vlijmen T, Mardones GA, Prabhu Y, Rojas AL, Mohammed S, Heck AJ, Raposo G, Van Der Sluijs P, Bonifacino JS (2008) Regulation of retromer recruitment to endosomes by sequential action of Rab5 and Rab7. *J Cell Biol* 183: 513–526
14. Seaman MNJ, Harbour ME, Tattersall D, Read E, Bright N (2009) Membrane recruitment of the cargo-selective retromer subcomplex is

- catalysed by the small GTPase Rab7 and inhibited by the Rab-GAP TBC1D5. *J Cell Sci* 122: 2371–2382
15. Seaman MNJ, Marcusson EG, Cereghino JL, Emr SD (1997) Endosome to golgi retrieval of the vacuolar protein sorting receptor, Vps10p, requires the function of the VPS29, VPS30, and VPS35 gene products. *J Cell Biol* 137: 79–92
  16. Burd C, Cullen PJ (2014) Retromer: a master conductor of endosome sorting. *Cold Spring Harb Perspect Biol* 6: a016774
  17. Steinberg F, Gallon M, Winfield M, Thomas EC, Bell AJ, Heesom KJ, Tavaré JM, Cullen PJ (2013) A global analysis of SNX27–retromer assembly and cargo specificity reveals a function in glucose and metal ion transport. *Nat Cell Biol* 15: 461–471
  18. Seaman MNJ (2012) The retromer complex – endosomal protein recycling and beyond. *J Cell Sci* 125: 4693–4702
  19. Harbour ME, Breusegem SYA, Antrobus R, Freeman C, Reid E, Seaman MNJ (2010) The cargo-selective retromer complex is a recruiting hub for protein complexes that regulate endosomal tubule dynamics. *J Cell Sci* 123: 3703–3717
  20. MCGOUGH IJ, Steinberg F, Gallon M, Yatsu A, Ohbayashi N, Heesom KJ, Fukuda M, Cullen PJ (2014) Identification of molecular heterogeneity in SNX27-retromer-mediated endosome-to-plasma-membrane recycling. *J Cell Sci* 127: 4940–4953
  21. Zhong Q, Watson MJ, Lazar CS, Hounslow AM, Waltho JP, Gill GN (2005) Determinants of the endosomal localization of sorting nexin 1. *Mol Biol Cell* 16: 2049–2057
  22. Kvainickas A, Jimenez Orgaz A, Nägele H, Hu Z, Dengjel J, Steinberg F (2017) Cargo-selective SNX-BAR proteins mediate retromer trimer independent retrograde transport. *J Cell Biol* 216: 3677–3693
  23. Simonetti B, Danson CM, Heesom KJ, Cullen PJ (2017) Sequence-dependent cargo recognition by SNX-BARs mediates retromer-independent transport of CI-MPR. *J Cell Biol* 216: 3695–3712
  24. MCGOUGH IJ, Cullen PJ (2011) Recent advances in retromer biology. *Traffic* 12: 963–971
  25. Helfer E, Harbour ME, Henriot V, Lakisic G, Sousa-Blin C, Volceanov L, Seaman MNJ, Gautreau A (2013) Endosomal recruitment of the WASH complex: active sequences and mutations impairing interaction with the retromer. *Biol Cell* 105: 191–207
  26. Zavodszky E, Seaman MNJ, Moreau K, Jimenez-Sanchez M, Breusegem SY, Harbour ME, Rubinsztein DC (2014) Mutation in VPS35 associated with Parkinson's disease impairs WASH complex association and inhibits autophagy. *Nat Commun* 5: 3828
  27. Gomez TS, Billadeau DD (2009) A FAM21-containing WASH complex regulates retromer-dependent sorting. *Dev Cell* 17: 699–711
  28. Derivery E, Sousa C, Gautier JJ, Lombard B, Loew D, Gautreau A (2009) The Arp2/3 activator WASH controls the fission of endosomes through a large multiprotein complex. *Dev Cell* 17: 712–723
  29. Seaman MNJ, Gautreau A, Billadeau DD (2013) Retromer-mediated endosomal protein sorting: all WASHed up!. *Trends Cell Biol* 23: 522–528
  30. Temkin P, Lauffer B, Jäger S, Cimermancic P, Krogan NJ, von Zastrow M (2011) SNX27 mediates retromer tubule entry and endosome-to-plasma membrane trafficking of signalling receptors. *Nat Cell Biol* 13: 715–721
  31. Steinberg F, Heesom KJ, Bass MD, Cullen PJ (2012) SNX17 protects integrins from degradation by sorting between lysosomal and recycling pathways. *J Cell Biol* 197: 219–230
  32. Hesketh GG, Pérez-Dorado I, Jackson LP, Wartosch L, Schäfer IB, Gray SR, McCoy AJ, Zeldin OB, Garman EF, Harbour ME et al (2014) VARP is recruited on to endosomes by direct interaction with retromer, where together they function in export to the cell surface. *Dev Cell* 29: 591–606
  33. McNally KE, Faulkner R, Steinberg F, Gallon M, Ghai R, Pim D, Langton P, Pearson N, Danson CM, Nägele H et al (2017) Retriever is a multiprotein complex for retromer-independent endosomal cargo recycling. *Nat Cell Biol* 19: 1214–1225
  34. Christoforidis S, Miaczynska M, Ashman K, Wilm M, Zhao L, Yip SC, Waterfield MD, Backer JM, Zerial M (1999) Phosphatidylinositol-3-OH kinases are Rab5 effectors. *Nat Cell Biol* 1: 249–252
  35. Christoforidis S, Zerial M (2000) Purification and identification of novel rab effectors using affinity chromatography. *Methods* 20: 403–410
  36. Fukuda M (2010) How can mammalian Rab small GTPases be comprehensively analyzed?: Development of new tools to comprehensively analyze mammalian Rabs in membrane traffic. *Histol Histopathol* 25: 1473–1480
  37. Gillingham AK, Sinka R, Torres IL, Lilley KS, Munro S (2014) Toward a comprehensive map of the effectors of rab GTPases. *Dev Cell* 31: 358–373
  38. Huttlin EL, Bruckner RJ, Paulo JA, Cannon JR, Ting L, Baltier K, Colby G, Gebreb F, Gygi MP, Parzen H et al (2017) Architecture of the human interactome defines protein communities and disease networks. *Nature* 545: 505–509
  39. Alanko J, Mai A, Jacquemet G, Schauer K, Kaukonen R, Saari M, Goud B, Ivaska J (2015) Integrin endosomal signalling suppresses anoikis. *Nat Cell Biol* 17: 1412–1421
  40. Pellinen T, Tuomi S, Arjonen A, Wolf M, Edgren H, Meyer H, Grosse R, Kitzing T, Rantala JK, Kallioniemi O (2008) Integrin trafficking regulated by Rab21 is necessary for cytokinesis. *Dev Cell* 15: 371–385
  41. Burgo A, Sotirakis E, Simmler M-C, Verraes A, Chamot C, Simpson JC, Lanzetti L, Proux-Gillardeaux VER, Galli T (2009) Role of Varp, a Rab21 exchange factor and TI-VAMP/VAMP7 partner, in neurite growth. *EMBO Rep* 10: 1117–1124
  42. Jean S, Cox S, Nassari S, Kiger AA (2015) Starvation-induced MTMR13 and RAB21 activity regulates VAMP8 to promote autophagosome-lysosome fusion. *EMBO Rep* 16: 297–311
  43. Drissi R, Dubois M-L, Douziech M, Boisvert F-M (2015) Quantitative proteomics reveals dynamic interactions of the minichromosome maintenance complex (MCM) in the cellular response to etoposide induced DNA damage. *Mol Cell Proteomics* 14: 2002–2013
  44. Simpson JC, Griffiths G, Wessling-Resnick M, Franssen JAM, Bennett H, Jones AT (2004) A role for the small GTPase Rab21 in the early endocytic pathway. *J Cell Sci* 117: 6297–6311
  45. Yuan Q, Ren C, Xu W, Petri B, Zhang J, Zhang Y, Kubes P, Wu D, Tang W (2017) PKN1 directs polarized RAB21 vesicle trafficking via RPH3A and is important for neutrophil adhesion and ischemia-reperfusion injury. *Cell Rep* 19: 2586–2597
  46. Martell JD, Deerinck TJ, Sancak Y, Poulos TL, Mootha VK, Sosinsky GE, Ellisman MH, Ting AY (2012) Engineered ascorbate peroxidase as a genetically encoded reporter for electron microscopy. *Nat Biotechnol* 30: 1143–1148
  47. Lee S-Y, Kang M-G, Shin S, Kwak C, Kwon T, Seo JK, Kim J-S, Rhee H-W (2017) Architecture mapping of the inner mitochondrial membrane proteome by chemical tools in live cells. *J Am Chem Soc* 139: 3651–3662
  48. Lee S-Y, Kang M-G, Park J-S, Lee G, Ting AY, Rhee H-W (2016) APEX fingerprinting reveals the subcellular localization of proteins of interest. *Cell Rep* 15: 1837–1847

49. St-Denis N, Gupta GD, Lin Z-Y, Gonzalez-Badillo B, Veri AO, Knight JDR, Rajendran D, Couzens AL, Currie KW, Tkach JM *et al* (2016) Phenotypic and interaction profiling of the human phosphatases identifies diverse mitotic regulators. *Cell Rep* 17: 2488–2501
50. Sönnichsen B, De Renzis S, Nielsen E, Rietdorf J, Zerial M (2000) Distinct membrane domains on endosomes in the recycling pathway visualized by multicolor imaging of Rab4, Rab5, and Rab11. *J Cell Biol* 149: 901–914
51. De Renzis S, Sönnichsen B, Zerial M (2002) Divalent Rab effectors regulate the sub-compartmental organization and sorting of early endosomes. *Nat Cell Biol* 4: 124–133
52. Choi H, Larsen B, Lin Z-Y, Breitzkreutz A, Mellacheruvu D, Fermin D, Qin ZS, Tyers M, Gingras A-C, Nesvizhskii AI (2010) SAINT: probabilistic scoring of affinity purification–mass spectrometry data. *Nat Methods* 8: 70–73
53. Knight JDR, Choi H, Gupta GD, Pelletier L, Raught B, Nesvizhskii AI, Gingras A-C (2017) ProHits-viz: a suite of web tools for visualizing interaction proteomics data. *Nat Methods* 14: 645–646
54. Jean S, Cox S, Schmidt EJ, Robinson FL, Kiger A (2012) Sbf/MTMR13 coordinates PI(3)P and Rab21 regulation in endocytic control of cellular remodeling. *Mol Biol Cell* 23: 2723–2740
55. De Franceschi N, Hamidi H, Alanko J, Sahgal P, Ivaska J (2015) Integrin traffic – the update. *J Cell Sci* 128: 839–852
56. Chotard L, Mishra AK, Sylvain M-A, Tuck S, Lambright DG, Rocheleau CE (2010) TBC-2 regulates RAB-5/RAB-7-mediated endosomal trafficking in *Caenorhabditis elegans*. *Mol Biol Cell* 21: 2285–2296
57. Fuchs E, Haas AK, Spooner RA, Yoshimura S-I, Lord JM, Barr FA (2007) Specific Rab GTPase-activating proteins define the Shiga toxin and epidermal growth factor uptake pathways. *J Cell Biol* 177: 1133–1143
58. Lobingier BT, Hüttenhain R, Eichel K, Miller KB, Ting AY, von Zastrow M, Krogan NJ (2017) An approach to spatiotemporally resolve protein interaction networks in living cells. *Cell* 169: 350–360.e12
59. Priya A, Kalaidzidis IV, Kalaidzidis Y, Lambright D, Datta S (2014) Molecular insights into Rab7-mediated endosomal recruitment of core retromer: deciphering the role of Vps26 and Vps35. *Traffic* 16: 68–84
60. Schindler C, Chen Y, Pu J, Guo X, Bonifacino JS (2015) EARP is a multi-subunit tethering complex involved in endocytic recycling. *Nat Cell Biol* 17: 639–650
61. Gershlick DC, Schindler C, Chen Y, Bonifacino JS (2016) TSSC1 is novel component of the endosomal retrieval machinery. *Mol Biol Cell* 27: 2867–2878
62. Rottner K, Hänisch J, Campellone KG (2010) WASH, WHAMM and JMY: regulation of Arp2/3 complex and beyond. *Trends Cell Biol* 20: 650–661
63. Shin H-W, Hayashi M, Christoforidis S, Lacas-Gervais S, Hoepfner S, Wenk MR, Modregger J, Uttenweiler-Joseph S, Wilm M, Nystuen A *et al* (2005) An enzymatic cascade of Rab5 effectors regulates phosphoinositide turnover in the endocytic pathway. *J Cell Biol* 170: 607–618
64. Muhammad E, Levitas A, Singh SR, Braiman A, Ofir R, Etzion S, Sheffield VC, Etzion Y, Carrier L, Parvari R (2015) PLEKHM2 mutation leads to abnormal localization of lysosomes, impaired autophagy flux and associates with recessive dilated cardiomyopathy and left ventricular noncompaction. *Hum Mol Genet* 24: 7227–7240
65. Shin C-S, Mishra P, Watrous JD, Carelli V, Aurelio MDR, Jain M, Chan DC (2017) The glutamate/cystine xCT antiporter antagonizes glutamine metabolism and reduces nutrient flexibility. *Nat Commun* 8: 1–11
66. Hao Y-H, Fountain MD Jr, Tacer KF, Xia F, Bi W, Kang S-HL, Patel A, Rosenfeld JA, Le Caignec C, Isidor B *et al* (2015) USP7 acts as a molecular rheostat to promote WASH-dependent endosomal protein recycling and is mutated in a human neurodevelopmental disorder. *Mol Cell* 59: 956–969
67. Udeshi ND, Pedram K, Svinkina T, Fereshetian S, Myers SA, Aygun O, Krug K, Clauser K, Ryan D, Ast T *et al* (2017) Antibodies to biotin enable large-scale detection of biotinylation sites on proteins. *Nat Methods* 14: 1167–1170
68. Pellinen T, Arjonen A, Vuoriluoto K, Kallio K, Fransén JAM, Ivaska J (2006) Small GTPase Rab21 regulates cell adhesion and controls endosomal traffic of beta1-integrins. *J Cell Biol* 173: 767–780
69. Ran FA, Hsu PD, Wright J, Agarwala V, Scott DA, Zhang F (2013) Genome engineering using the CRISPR-Cas9 system. *Nat Protoc* 8: 2281–2308
70. Hao Y-H, Doyle JM, Ramanathan S, Gomez TS, Jia D, Xu M, Chen ZJ, Billadeau DD, Rosen MK, Potts PR (2013) Regulation of WASH-dependent actin polymerization and protein trafficking by ubiquitination. *Cell* 152: 1051–1064
71. Seaman MNJ (2009) Enhanced snapshot: endosome-to-golgi retrieval. *Cell* 139: 1198.e1
72. Maldonado-Báez L, Williamson C, Donaldson JG (2013) Clathrin-independent endocytosis: a cargo-centric view. *Exp Cell Res* 319: 2759–2769
73. Eyster CA, Higginson JD, Huebner R, Porat-Shliom N, Weigert R, Wu WW, Shen R-F, Donaldson JG (2009) Discovery of new cargo proteins that enter cells through clathrin-independent endocytosis. *Traffic* 10: 590–599
74. Maldonado-Báez L, Cole NB, Krämer H, Donaldson JG (2013) Microtubule-dependent endosomal sorting of clathrin-independent cargo by Hook1. *J Cell Biol* 201: 233–247
75. Kvainickas A, Orgaz AJ, Nägele H, Diedrich B, Heesom KJ, Dengjel J, Cullen PJ, Steinberg F (2017) Retromer- and WASH-dependent sorting of nutrient transporters requires a multivalent interaction network with ANKRD50. *J Cell Sci* 130: 382–395
76. Zhang X (2006) Varp is a Rab21 guanine nucleotide exchange factor and regulates endosome dynamics. *J Cell Sci* 119: 1053–1062
77. Simonsen A, Lippé R, Christoforidis S, Gaullier JM, Brech A, Callaghan J, Toh BH, Murphy C, Zerial M, Stenmark H (1998) EEA1 links PI(3)K function to Rab5 regulation of endosome fusion. *Nature* 394: 494–498
78. Kim DI, Cutler JA, Na CH, Reckel S, Renuse S, Madugundu AK, Tahir R, Goldschmidt HL, Reddy KL, Hugarin RL *et al* (2018) BioSITe: a method for direct detection and quantitation of site-specific biotinylation. *J Proteome Res* 17: 759–769
79. Derivery E, Gautreau A (2010) Assaying WAVE and WASH complex constitutive activities toward the Arp2/3 complex. *Methods Enzymol* 484: 677–695
80. Gomez TS, Gorman JA, Artal-Martinez De Narvajás A, Koenig AO, Billadeau DD (2012) Trafficking defects in WASH-knockout fibroblasts originate from collapsed endosomal and lysosomal networks. *Mol Biol Cell* 23: 3215–3228
81. Harterink M, Port F, Lorenowicz MJ, Mcgough IJ, Silhankova M, Betist MC, van Weering JRT, Heesbeen RGHPV, Middelkoop TC, Basler K *et al* (2011) A SNX3-dependent retromer pathway mediates retrograde transport of the Wnt sorting receptor Wntless and is required for Wnt secretion. *Nat Cell Biol* 13: 914–923
82. Jia D, Gomez TS, Billadeau DD, Rosen MK (2012) Multiple repeat elements within the FAM21 tail link the WASH actin regulatory complex to the retromer. *Mol Biol Cell* 23: 2352–2361
83. Buckley CM, Gopaldass N, Bosmani C, Johnston SA, Soldati T, Insall RH, King JS (2016) WASH drives early recycling from macropinosomes and phagosomes to maintain surface phagocytic receptors. *Proc Natl Acad Sci USA* 113: E5906–E5915

84. Koronakis V, Hume PJ, Humphreys D, Liu T, Hørning O, Jensen ON, McGhie EJ (2011) WAVE regulatory complex activation by cooperating GTPases Arf and Rac1. *Proc Natl Acad Sci USA* 108: 14449–14454
85. Lebensohn AM, Kirschner MW (2009) Activation of the WAVE complex by coincident signals controls actin assembly. *Mol Cell* 36: 512–524
86. Donaldson JG, Johnson DL, Dutta D (2016) Rab and Arf G proteins in endosomal trafficking and cell surface homeostasis. *Small GTPases* 7: 247–251
87. Dutta D, Donaldson JG (2015) Sorting of clathrin-independent cargo proteins depends on Rab35 delivered by clathrin-mediated endocytosis. *Traffic* 16: 994–1009
88. Shin JJH, Gillingham AK, Begum F, Chadwick J, Munro S (2017) TBC1D23 is a bridging factor for endosomal vesicle capture by golgins at the trans-Golgi. *Nat Cell Biol* 19: 1424–1432
89. Dubois M-L, Bastin C, Lévesque D, Boisvert F-M (2016) Comprehensive characterization of minichromosome maintenance complex (MCM) protein interactions using affinity and proximity purifications coupled to mass spectrometry. *J Proteome Res* 15: 2924–2934
90. Lam SS, Martell JD, Kamer KJ, Deerinck TJ, Ellisman MH, Mootha VK, Ting AY (2014) Directed evolution of APEX2 for electron microscopy and proximity labeling. *Nat Methods* 12: 51–54
91. Jean S, Kiger AA (2016) RAB21 activity assay using GST-fused APPL1. *Bio Protoc* 6: e1738
92. Guan X, Rastogi N, Parthun MR, Freitas MA (2014) SILAC peptide ratio calculator: a tool for SILAC quantitation of peptides and post-translational modifications. *J Proteome Res* 13: 506–516
93. Liu G, Zhang J, Larsen B, Stark C, Breitkreutz A, Lin Z-Y, Breitkreutz B-J, Ding Y, Colwill K, Pasculescu A et al (2010) ProHits: integrated software for mass spectrometry– based interaction proteomics. *Nat Biotechnol* 28: 1015–1017
94. Tyanova S, Temu T, Sinitcyn P, Carlson A, Hein MY, Geiger T, Mann M, Cox J (2016) The Perseus computational platform for comprehensive analysis of (prote)omics data. *Nat Methods* 13: 731–740
95. Carpenter AE, Jones TR, Lamprecht MR, Clarke C, Kang IH, Friman O, Guertin DA, Chang JH, Lindquist RA, Moffat J et al (2006) Cell Profiler: image analysis software for identifying and quantifying cell phenotypes. *Genome Biol* 7: R100
96. Sullender M, Hegde M, Vaimberg EW, Donovan KF, Smith I, Tothova Z, Wilen C, Orchard R, Virgin HW, Doench JG et al (2016) Optimized sgrNA design to maximize activity and minimize off-target effects of crispr-cas9. *Nat Biotechnol* 34: 184–191
97. Jimenez Orgaz A, Kvainickas A, Nägele H, Denner J, Eimer S, Dengjel J, Steinberg F (2018) Control of RAB7 activity and localization through the retromer-TBC1D5 complex enables RAB7-dependent mitophagy. *EMBO J* 37: 235–254